NUMERICAL SIMULATIONS OF BUBBLE PUMPS FOR DIFFUSION-ABSORPTION REFRIGERATION

By

SOO W. JO

A THESIS PRESENTED TO THE GRADUATE SCHOOL
OF THE UNIVERSITY OF FLORIDA IN PARTIAL FULFILLMENT
OF THE REQUIREMENTS FOR THE DEGREE OF
MASTER OF SCIENCE

UNIVERSITY OF FLORIDA

2012

To my parents

ACKNOWLEDGMENTS

First of all, I would like to offer my sincere gratitude to Prof. Sherif and Prof. Lear for serving as my advisor and co-advisor, respectively. This work could not have been finished if it were not for their guidance with valuable advices. I also would like to acknowledge their insightful comments which helped me to improve the quality of this thesis.

In addition, I would like to thank Mr. Lee who is my CFX instructor for giving me assistances in revising the grids appropriately so that the simulations could have been run properly.

Lastly, I sincerely thank my parents for their infinite love and support. I could never be where I am right now without all the love and support that they have given to me. It is truly indescribable how blessed and lucky I am to have them.

TABLE OF CONTENTS

LIST OF TABLES

LIST OF FIGURES

NOMENCLATURE

$A_{\alpha\beta}$	interfacial contact area
$h_{\alpha\beta}$	heat transfer coefficient for particle
$\Gamma_{\alpha\beta}$	mass flow rate per unit volume from phase-β to phase-α
$H_{\alpha s}$	interfacial enthalpy transfer to phase-α
$q_{\alpha s}$	sensible heat flux to phase-α from the interface
$\dot{m}_{\alpha\beta}$	mass flux into phase-α from phase-β
d	diameter
L	length
P_{in}	inlet pressure
q_w	wall heat flux
Φ_{in}	inlet mass flux

Abstract of Thesis Presented to the Graduate School
of the University of Florida in Partial Fulfillment of the
Requirements for the Degree of Master of Science

NUMERICAL SIMULATIONS OF BUBBLE PUMPS FOR DIFFUSION-ABSORPTION REFRIGERATION

By

SOO W. JO

May 2012

Chair: S. A. Sherif
Co-Chair: William E. Lear
Major: Mechanical Engineering

A bubble pump is a key component for diffusion-absorption refrigeration systems operating at a single pressure. Nevertheless, research focusing on bubble pumps is not widely found in the literature.

In this study, a bubble pump model with a shape of vertical tube subjected to a uniform heat flux from the tube outer surface is numerically simulated. A saturated ammonia-water solution enters the bubble pump inlet and receives heat from the pump wall along the entire pump length. During the process, most of ammonia in the solution vaporizes, and the remaining solution is lifted by the buoyant force created by the ammonia vapor. A numerical model was implemented by employing a commercial CFD code. The applicability of the numerical model implemented in the code to the present numerical simulations was validated through a comparative study referring to experimental data of a boiling phase change flow of water in a vertical pipe being subjected to a uniform heat flux.

To investigate the influence of the bubble pump's geometrical dimension and the heat input on the operating status and performance, numerical simulations were

performed for four bubble pumps with different diameters subjected to five amounts of heat flux. Simulation results were provided in terms of the flow parameters including void fraction, and vapor and liquid velocities.

The simulated spatial distributions of the flow parameters were found to have steep gradients in the radial direction near the pump wall due to the heating from the pump wall. In addition, simulated flow parameters were compared to those in previous one-dimensional (1-D) work for the same problem. It was found that the void fraction profiles along the pump length simulated in this study seem to be similar to those in 1-D models, but somewhat different quantitatively.

Based on the results, the present numerical simulation model of the bubble pump can be useful for certain industrial applications, but inaccuracy exists in the simulations. Currently, the accuracy of the simulations could not be assessed precisely because there are insufficient experimental data for bubble pumps to compare with. Therefore, supporting experimental tests need to be done in the future for evaluating the present numerical model.

CHAPTER 1
INTRODUCTION AND BACKGROUND

The motivation of this study was driven by an application of renewable energy sources. Conventional energy sources such as petroleum, coal, and natural gas will not last long. Therefore, the need to make use of renewable energy such as solar, geothermal, and wind has been long sought. Solar energy is one of the most widely available renewable energy sources. About 3,850,000 exajoules (EJ) of solar energy is received by earth every year. It is estimated that earth gets more energy from the sun in an hour than the world uses in a year. Unlike most other energy sources, solar energy can be obtained everywhere around the world. Petroleum, coal, natural gas, tidal power, wave power, etc. are found in limited regions around the world, so the delivery of these energy sources to end users by means of transportation and infrastructure is necessary. However, neither transportation nor infrastructure is needed for solar energy since it can be acquired anywhere on site.

There are various applications of solar energy. The subject of interest in this study is solar-assisted refrigeration. Such systems can be powered by solar thermal collectors or solar photovoltaic panels. Thermal energy can power absorption or adsorption refrigeration systems, while electric energy from photovoltaic systems can power standard vapor compression refrigerators. Typically, absorption refrigeration systems are smaller than adsorption systems in terms of physical dimensions for the same refrigeration capacity because of the high heat transfer coefficient of the absorbent. This study addresses numerical simulations of bubble pump, which is one of the key components of an absorption refrigeration system powered by solar thermal collectors.

Absorption Refrigeration

The process of attracting and holding moisture by desiccants is defined as absorption. This process has been most commonly employed for solar thermal refrigeration cycles. A heat source is needed to supply thermal energy for operating an absorption system. Other sources of thermal energy such as geothermal and waste energy from turbines or other industrial processes can also be used. Conventional vapor compression refrigerators use electricity supplied by power plants via the electricity grid. Due to this restriction, vapor compression refrigerators cannot generally be used in undeveloped locations in the Third World. Absorption refrigerators are free of such limitations as their energy source is everywhere around the world. Besides, vapor compression refrigerators typically use environmentally unfriendly refrigerants, which either contribute to the depletion of the ozone layer or the increase of greenhouse gases. Absorption refrigerators do not cause such problems.

History

The development of absorption refrigeration began in the 18th century. It was discovered that evaporating pure water from a vessel contained within an evacuated vessel holding sulfuric acid generates ice. This phenomenon occurs because a reduction in temperature is caused by the absorption of water by the acid.

Edmond Carré developed the first absorption refrigerator with water and sulfuric acid in 1850 [1]. Later in 1858, an absorption refrigerator employing ammonia and water as working fluids was developed by Ferdinand Carré who is Edmond Carré's brother. Several new equipment adopted this concept to make ice and store food.

In 1922, a diffusion-absorption refrigerator was invented by Baltzar von Platen and Carl Munters who were students at the Royal Institute of Technology in Sweden [2].

This absorption refrigerator, often called the Platen-Munters cycle, operates at a single pressure. It can work without a compressor, thus eliminating the need for mechanical work. Typical absorption-diffusion systems use ammonia, water, and hydrogen gas which represent a refrigerant, an absorbent, and an auxiliary gas, respectively, for their working fluids. Production of this single-pressure absorption refrigerator began in 1923 by AB Arctic, and the Platen-Munters refrigerator was patented in 1928.

An alternative design of an absorption refrigerator operating at a single pressure was invented by Albert Einstein and Leó Szilárd in 1926 [3]. This design differs from the Platen-Munters cycle because a pressure-equalizing fluid is used instead of an auxiliary gas. The Einstein refrigerator uses butane, water, and ammonia which represent a refrigerant, an absorbent, and a pressure-equalizing fluid, respectively as their working fluids. Unlike diffusion-absorption refrigeration, a condenser and an absorber were consolidated into a single component in the Einstein refrigerator. This technology was patented in 1930.

The absorption refrigeration market flourished until the mid 1970s, but the low cost of electricity favoring vapor compression refrigerators restrained its growth. Nevertheless, diffusion-absorption refrigeration technology is still being used for refrigerators in recreational vehicles or hotel rooms.

Mechanism

There are various types of absorption refrigerators. In this study, diffusion-absorption refrigerators (DARs) [2] which have been used for many years as domestic refrigerators are investigated in detail. Diffusion-absorption refrigerators (DARs) are quite different from conventional vapor compression refrigerators. The former do not compress the refrigerant, so they operate at a fairly constant single pressure. A

compressor is used to circulate the refrigerant in vapor compression refrigerators, so they operate at dual pressures. A schematic of a diffusion-absorption refrigeration cycle working under a single pressure is shown in Figure 1-1.

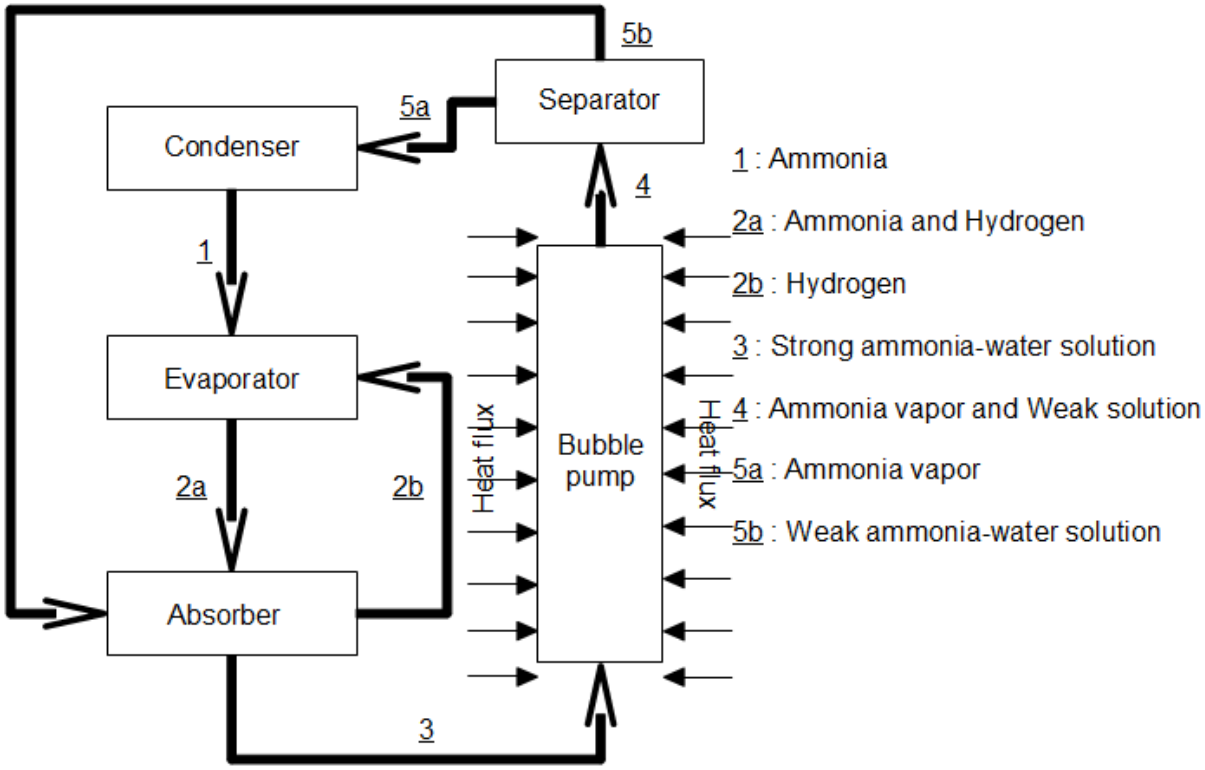

Figure 1-1. Diffusion-absorption refrigeration cycle.

In diffusion-absorption refrigerators, the refrigerant is circulated by thermal energy instead of mechanical energy. First, the ammonia liquid is mixed with the hydrogen gas in the evaporator. In this process, the total pressure reduction triggers the vaporization of the ammonia liquid. When the ammonia liquid vaporizes, it takes heat away from the surroundings to provide cooling. The mixture of ammonia vapor and the hydrogen gas is sent to the absorber where the weak ammonia-water solution (low in ammonia concentration) is injected to separate the ammonia vapor from the hydrogen gas. Hydrogen gas is sent back to the evaporator while the strong ammonia-water solution

(high in ammonia concentration) is sent to the bubble pump where the added heat boils it. Consequently, ammonia is vaporized from the ammonia-water solution since the boiling temperature of ammonia is lower than that of the water. While the ammonia vapor leaves the bubble pump through the top outlet from boiling, the weak ammonia-water solution also leaves through the top outlet along with the ammonia vapor. The separator filters the weak ammonia-water solution away from the ammonia vapor. Then the weak ammonia-water solution is sent back to the absorber and the ammonia vapor is sent to the condenser. The amount of mechanical energy used in this absorption refrigeration system is zero as explained above. Using the bubble pump, it is possible to operate an absorption refrigerator with only thermal energy.

Refrigerants and Absorbents

It is known that about 40 refrigerants and 200 absorbents are available as working fluids for absorption refrigeration processes. The most usual pair of working fluids is water and ammonia in which case water is the absorbent and ammonia is the refrigerant. Also, the pair of lithium-bromide and water in which lithium-bromide is the absorbent and water is the refrigerant is often found. In general, the working fluids for absorption refrigeration need to have the following characteristics.

- The refrigerant needs to have a high heat of vaporization and a good solubility in the absorbent.
- The boiling temperature difference between the refrigerant and the solution should be large enough to achieve high thermodynamic efficiency.
- The refrigerant and absorbent should be environmentally friendly and non-corrosive.

Bubble Pump

The bubble pump is simply a vertical tube which lifts up the fluid by increasing the buoyancy of the fluid under two-phase flow conditions. Bubbles that are generated inside the bubble pump reduce the hydrostatic pressure over the length of the bubble pump. Phase change from liquid to vapor increases the buoyancy of the fluid which enables it to rise. The generation of bubbles comes from applying heat to the tube from a thermal energy source. A practical application of bubble pumps used in daily life is the coffee percolator in which the vaporized liquid at the percolator surface rises in a vertical tube to the top while brewing coffee. Bubble pumps exist in different configurations. They can be a single vertical tube in which heat flux is applied to only a small region near the inlet, or over the entire length. The refrigerating capacity of the system can be increased by setting up multiple bubble pumps in parallel which increases the flow rate of the refrigerant. Heat transfer into bubble pumps can be done directly by projecting sunlight onto the surface, or indirectly by utilizing a heat exchanger.

CHAPTER 2
LITERATURE REVIEW

The history of absorption refrigeration began in the early 1900s, so research in this area is well documented. However, research in bubble pumps is not widely available in the literature. Most articles investigating bubble pumps have been published in the last couple of decades.

White [4] performed an experimental study of bubble pumps, and her experimental data were compared to five existing two-phase flow models in one dimension. Her objective was to determine the best two-phase flow model, and to use that model to perform parametric studies in order to determine the highest efficiency under different operating conditions. She programmed each model using the Engineering Equation Solver program and concluded that de Cachard and Delhaye's model [5] was the best fit. She found that the efficiency is not dependent on the length of the bubble pump, but is sensitive to the submergence ratio. This is the ratio of liquid level in the bubble pump to the bubble pump's length. She remarked that the optimum condition for operating a bubble pump occurs in the slug flow region, and reported on the existence of an ideal diameter for maximizing the efficiency. However, she commented that there was a lower boundary for the diameter depending on the ammonia-water solution flow rate to prevent a rapid drop in efficiency.

Shelton et al. [6] published an article based on White's work [4]. But unlike White [4], no experimental study was conducted. They developed a theoretical model based on the work of White [4] for the optimization of a small bubble pump in single pressure absorption refrigeration cycles, and conducted a parametric study to find the maximum efficiency under different operating conditions. Koyfman et al. [7] noted that White [4]

did not simulate the actual operating conditions of a bubble pump correctly because White [4] used an airlift pump for the experimental analysis of the system due to its simple setup. Koyfman et al. [7] built an experimental system that could operate continuously at the desired pressure level, and chose dimethylacetamide solvent and chlorodifluoromethane refrigerant as working fluids. They found that low potential heat sources such as solar energy may be utilized for absorption refrigeration.

Sathe [8] performed similar research to that of White [4] by building an experimental bubble pump in which heat is only applied at the inlet region. He used methanol for the working fluid, and tested the experimental bubble pump for different heat inputs, pump diameters, and driving heads at constant ambient pressure. Sathe [8] found that increasing the heat input increases the frequency of pumping action as well as the mass flow rate of both the vapor and liquid. He noted that the mass flow rate of the liquid increases by increasing the heat input, but decreases with an excessive heat input.

Dammak et al. [9] studied optimizing geometrical parameters of a solar bubble pump, which was integrated with a solar thermal collector using ammonia and water as the working fluids along with helium as the auxiliary gas. They conducted a theoretical analysis using the mathematical models developed by Shelton et al. [6], and proposed optimal values for the diameter, length, inclination angle, and submergence ratio of a bubble pump.

Benhmidene et al. [10] investigated on modeling a bubble pump in one dimension with ammonia and water as the working fluids. They simulated the operation of a bubble pump that is 1 m long with different diameters and mass flow rates using a one-

dimensional two-phase model. They determined the maximum liquid velocity over a range of heat flux for known diameters and mass flow rates, and derived an expression for the heat flux as a function of the diameter and mass flow rate.

Benhmidane et al. [11] conducted another study on simulating bubble pumps using ammonia and water as the working fluids. They simulated the performance numerically and developed a two-phase model to conduct one-dimensional (1-D) analysis of flow patterns in a bubble pump with the heat flux ranging from 5 kW/m² to 25 kW/m² with 5 kW/m² increments and different tube diameters from 6 mm to 12 mm with 2 mm increments. They constructed void fraction profiles and liquid/vapor velocity profiles using their numerical data.

Some of the previous theoretical studies on bubble pumps treated the system as a lumped model while others treated the system as a one-dimensional model. However, the previous theoretical studies on bubble pumps reviewed in this chapter have not fully validated their theoretical models of bubble pump with experimental data due to the unavailability of realistic bubble pump experimental models to compare with.

CHAPTER 3
MOTIVATION AND OBJECTIVES

To better understand the realistic operations of a bubble pump, a new improved method to conduct research on bubble pumps is desirable. The most ideal method would be building an actual bubble pump that boils a binary solution of ammonia and water, and then experimenting with it. Unfortunately, this approach is not feasible with limited resources. Even if a bubble pump is actually constructed, there would be problems with measuring the physical parameters of the working fluids inside the bubble pump. Alternatively, theoretical approaches can be employed. Most theoretical analyses of bubble pumps have been done with 1-D models. Therefore, it would be meaningful to study other numerical models using any of available commercial codes for more realistic simulation.

The objective of this research is to employ a numerical model for simulating multi-phase flows in bubble pumps. The numerical model is implemented by employing a commercial computational fluid dynamics (CFD) code that is well tested and commonly used worldwide. Operating conditions and physical configurations of the bubble pumps defined for the simulations are the same as those defined by Benhmidene et al. [11], and they are provided in the next chapter.

CHAPTER 4
NUMERICAL SIMULATION MODEL AND METHOD

The numerical simulation model and method applied for the present study on bubble pumps are described in this chapter.

Problem Statement

A bubble pump is a vertical tube in which a strong ammonia-water solution entering through the inlet at the bottom boils due to the heat applied to the tube's outer surface. Because the boiling temperature of water at a specified pressure condition is much higher than that of ammonia, only ammonia vaporizes from the saturated ammonia-water solution when the solution is heated.

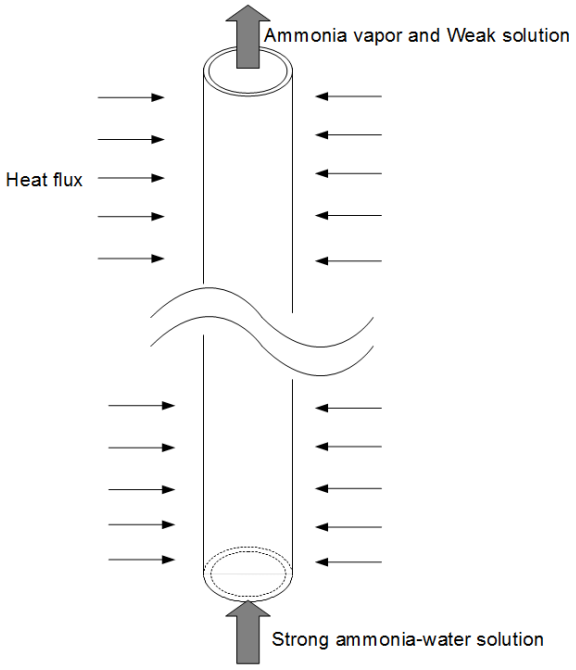

Figure 4-1. Schematic of a bubble pump

During the heating process, the strong ammonia-water solution that is high in ammonia concentration transforms to a weak ammonia-water solution that is low in ammonia concentration by generating ammonia vapor. This causes an increase in the boiling temperature of the weak solution and creates a buoyancy force. A schematic of

the bubble pump is shown in Figure 4-1.The problem defined in this study is the same as that addressed in Benhmidene et al. [11]. Four bubble pumps with different diameters are studied. The geometrical dimensions of the pumps named Pump A, Pump B, Pump C, and Pump D are shown in Table 4-1. The operating conditions defined for the simulations are shown in Table 4-2.

Table 4-1. Geometrical data of the bubble pumps

	Inside Diameter [mm]	Length [mm]
Pump A	6	1,000
Pump B	8	1,000
Pump C	10	1,000
Pump D	12	1,000

Table 4-2. Operating conditions for the simulations

Parameter [unit]	Value(s)
Heat flux [kW/m²]	5, 10, 15, 20, 25
Mass flux [kg/m²s]	20
Ammonia concentration at the inlet	0.4
Inlet pressure [bar]	18

As in the 1-D work by Benhmidene et al. [11], the ammonia-water solution is assumed to be in saturated state at the inlet of the bubble pump. The submerged zone in the tube where the binary solution is heated up to its saturation temperature without boiling is neglected.

Governing Equations

The governing transport equations for conservation of mass, momentum, energy, and turbulent quantities are solved to analyze multi-phase flow by employing one of the most widely used commercial CFD codes called ANSYS CFX [12]. The transport

equations in a Cartesian coordinate system for the present problem can be found in the literature [12]. In the present simulations, phase dependent turbulent models are used to calculate the turbulent viscosity μ_t of each phase. It is widely known that a two-equation model such as the k-epsilon model or shear stress transport (SST) model is recommended to use for continuous phases, while the zero-equation algebraic (eddy viscosity) turbulence model is recommended to use for dispersed phases [12]. The standard K-epsilon turbulence model is known to be the most widely used two-equation model with the Boussinesq hypothesis for predicting turbulent flows in industrial piping systems [12-15]. It is also known that the model is useful for free-shear layer flows with relatively small pressure gradients and its accuracy is reduced for flows containing large adverse pressure gradients.

For the present numerical simulations of dilute dispersed two-phase flows in bubble pumps, both the standard k-epsilon turbulence model and the algebraic turbulence model were used for the continuous liquid phase and dispersed gas phase flows, respectively, as recommended in reference [12]. The k-epsilon model is mainly valid for turbulent core flows, so the wall function approach is necessary [16, 17]. The wall function (semi-empirical function) method is used to treat the boundary layer in the near-wall region based on law of the wall for computational efficiency. It is well known that the wall functions can be used to provide near-wall boundary conditions for the momentum and turbulence transport equations [12-15]. Therefore, the viscous boundary layer does not have to be solved and the need for a very fine mesh is avoided so that the computational cost can be reduced significantly. However, using the k-epsilon model with the wall function method is known to cause considerable error for

wall boiling due to a modified transport of momentum and energy, and no simple fix is generally available to improve the accuracy.

Thermal Phase Change Model

The present calculation of multiphase flow accompanying thermal phase change employs a simple thermal phase change model. The saturated strong ammonia-water solution generates ammonia vapor due to heating, and it becomes a saturated weak solution at an elevated temperature. Thus, the following bulk boiling model option is implemented in the CFD code [12].

The source of volumetric mass for the interphase transfer processes is expressed in terms of mass fluxes as below where α can be vapor and β can be liquid.

$$\Gamma_{\alpha\beta} = A_{\alpha\beta}\dot{m}_{\alpha\beta}$$

The mass flux into phase-α from phase-β, $\dot{m}_{\alpha\beta}$ is given as,

$$\dot{m}_{\alpha\beta} = \frac{q_{\alpha s}+q_{\beta s}}{H_{\beta s}-H_{\alpha s}}$$

where $q_{\alpha s}$ and $q_{\beta s}$ are the sensible heat flux from the interface to phase-α and phase-β, respectively. $H_{\alpha s}$ and $H_{\beta s}$ represent the interfacial values of enthalpy carried into and out of the phases due to phase change, respectively. The properties of the ammonia-water binary solution are not available in the CFX code, so they are provided in the materials library of the code. The ammonia-water solution is configured as a variable composition mixture of saturated ammonia liquid and compressed (sub-cooled) water at 18 bar, and the properties of each of these two liquids are taken from the REFPROP program developed by NIST [18].

Since the latent heat of vaporization and the saturation temperatures over the range of varying ammonia concentration for the ammonia-water solution are not

available, these data are read from the 2009 ASHRAE Handbook Fundamentals [19] and are imported into the user function section in the code. As the analysis is performed under steady-state conditions, all the physical properties are considered to be independent of time.

Simulation Domain

As the bubble pump under consideration has a shape of a vertical tube, it is axial symmetric with respect to the centerline. Thus, the gradients of flow parameters can be assumed to be zero in the circumferential direction. This enables a simplification of the simulation model as a sliced arc column as shown in Figure 4-2. Then, a symmetrical boundary condition is placed on the two sliced faces to replicate an entire vertical tube.

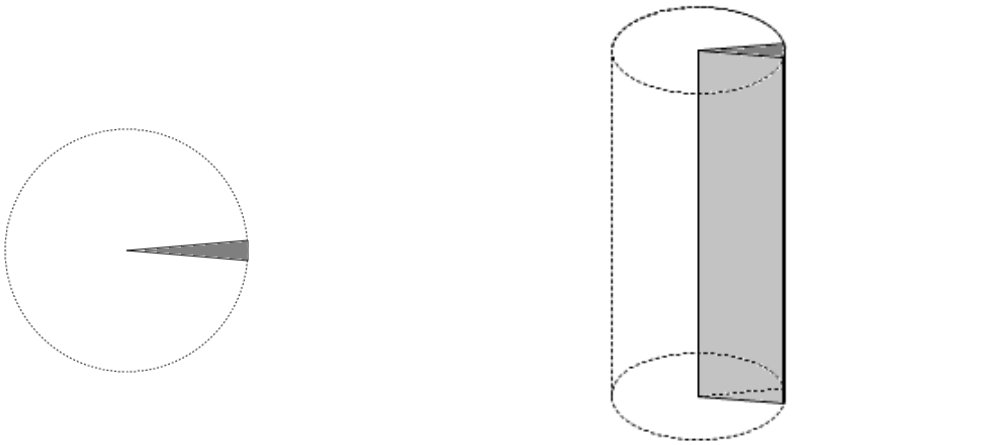

A B

(Note that the figures are not drawn to scale.)

Figure 4-2. Schematic of simplified simulation model. A) Top view. B) Isometric view.

The sliced arc column is 1/180 of the original tube, so the angle between two sides of the sliced arc column is 2°. This simplification does not affect the numerical simulation results because the present numerical model is not to microscopically simulate the boiling phenomena including the process of bubble creation and behavior

at the heated wall, but to globally calculate the distribution of void fraction of the fluid experiencing its phase change in the bubble pump.

A total of four geometries with different inside diameters are considered. For convenience, bubble pumps of 6 mm, 8 mm, 10 mm, 12 mm inside diameters are named Pump A, Pump B, Pump C, and Pump D, respectively, as in Table 4-1.

Boundary Conditions

Boundary surfaces are prescribed as shown in Figure 4-3.

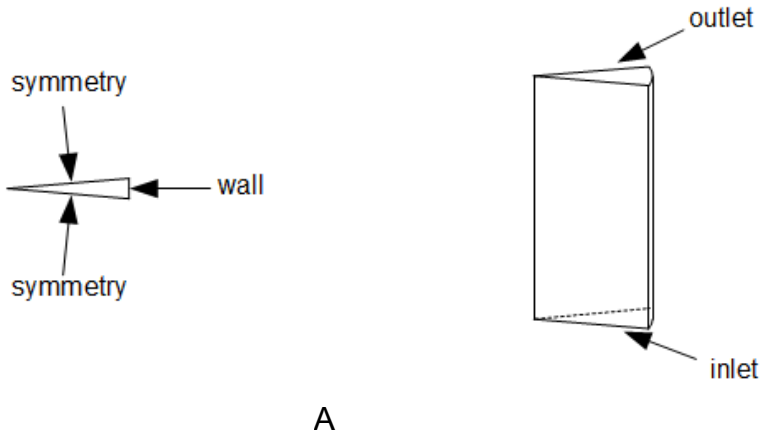

Figure 4-3. Boundary surfaces for the simulation models. A) Top view. B) Isometric view.

- At the inlet, the mass flux is given as defined by the operating conditions in Table 4-2. The flow temperature at the inlet is set to be 107°C which is the saturated liquid temperature of the ammonia-water solution at 40% ammonia concentration. Thus, only the saturated liquid phase of the solution would be present at the inlet as defined in the problem statement.

- At the outlet, the constant pressure boundary condition and the zero gradient condition for other variables are specified, and the velocities of all phases at the outlet boundary are adjusted to satisfy the mass conservation at each iteration level.

- At both symmetric surfaces, the boundary imposes zero normal gradient conditions. Also, the symmetrical boundary imposes free slip and adiabatic conditions.

- At the wall, a constant and uniform heat flux is applied on the wall surface. A no slip boundary condition is imposed on the wall, and the wall function method is used to treat the near-wall region. The wall thickness is assumed to be negligible in the simulations.

Discretization of Simulation Domain

The spatial domain created in the previous section is discretized into finite control volumes in the radial and longitudinal directions. This is only because the arc length of the selected domain is too small to be discretized further in the circumferential direction. Most mesh elements retain a hexahedra shape, but the ones located along the arc tip retain a wedge shape. The whole domain is discretized into fine enough meshes to get satisfactory mesh-independent results. To do this, the lengths of radial and longitudinal edges of a uniformly discretized element are set to about 0.15 mm and 1 mm, respectively. The assessment of mesh refinement is done later in order to ensure that the meshes are fine enough not to affect the void fraction, or the vapor or liquid velocities.

Numerical Solution Schemes

The governing equations are integrated over each control volume of the element such that the relevant quantities of mass, momentum, energy, etc. are conserved for each control volume. By using the finite volume method, the discrete conservation equations in the form of a linear set of equations are obtained and assembled into the solution matrix. For the CFD calculations of steady-state problems, the time-step behaves like an acceleration parameter to guide to a steady-state solution.

The iterative computation for each time step terminates automatically when the maximum of the absolute sum of dimensionless residuals of momentum, energy, or pressure correction equations is less than 0.0001. The iterative residual values of

momentum and mass, heat transfer, turbulence, and volume fractions are checked during the iterations to see if they are not diverging. Additionally, the imbalances of mass, momentum, and energy are monitored to ensure that they all converge to 0.

CHAPTER 5
VALIDATION OF NUMERICAL MODEL

In this chapter, both mesh independence and validation of the numerical model are performed in order to ensure that the numerical simulations produce practical results. The mesh independence test is performed first to see if the grid quality is high enough not to affect the flow field expressed in terms of void fraction, and vapor and liquid velocities. Subsequently, validation of the numerical model is performed by conducting simulations of a subcooled boiling flow in a vertical pipe subjected to a uniform wall heat flux for which the experimental data are available.

Mesh Independence Test

Results of the simulations should not be affected by the mesh density, so it is necessary to conduct a test for grid independence. Mesh independence tests were performed in reference [20] for the numerical simulation of the boiling phase change flow in the vertical heated pipe with a diameter of 12 mm and a length of 2 m, which is similar to the present bubble Pump D except for the fluid and the pipe length. The tests in reference [20] with three different meshes of 20(number of radial elements)X150(number of longitudinal elements), 40X300 and 80X600 showed that there was little difference in the calculation results in terms of the cross-sectional area averaged void fraction and liquid temperature.

Based on the mesh independence tests [20], the original mesh properties of Pumps A, B, C, and D are designed for the present numerical simulations as in Table 5-1.

Table 5-1. Number of mesh elements

	Number of radial elements	Number of longitudinal elements	Total number of body elements
Pump A	20	1000	20000
Pump B	27	1000	27000
Pump C	33	1000	33000
Pump D	40	1000	40000

Views of Pump A mesh and Pump D mesh are given as examples for better visualization of meshes. Figures 5-1 and 5-2 show isometric and top views of the Pump A and Pump D meshes, respectively.

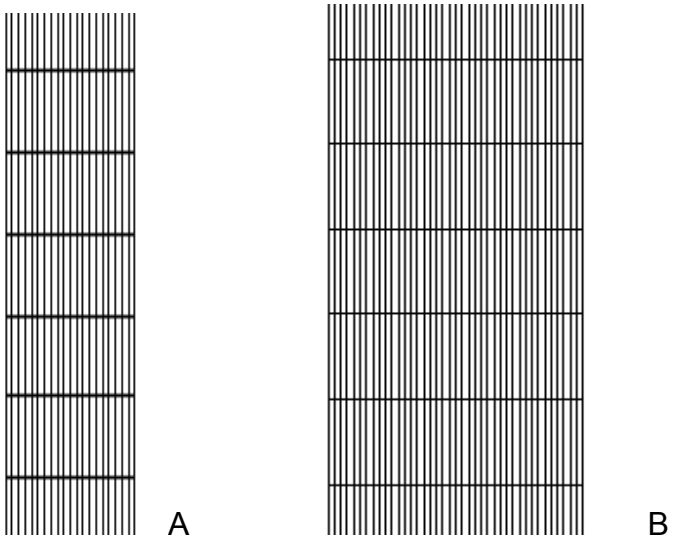

Figure 5-1. Front mesh views. A) Pump A. B) Pump D.

Figure 5-2. Top mesh views. A) Pump A. B) Pump D.

To see if the grid size defined above is sufficiently fine, a finer mesh was generated for Pump A with the grid size on the radial and longitudinal edges equal to half of the original grid size. This makes the finer mesh to be four times denser than the original mesh. Therefore, the finer mesh has 40 radial edge elements and 2000 longitudinal edge elements making up 80000 total body elements. Trial simulations were run on both the original Pump A mesh and the finer Pump A mesh at a heat flux of 5 kW/m² or 25 kW/m². The void fraction and the vapor and liquid velocities between the original mesh and the finer mesh are shown in Figures 5-3 through 5-5, respectively.

As seen in Figures 5-3 through 5-5, both the original Pump A mesh and the finer Pump A mesh yield almost the same data either at a heat flux of 5 kW/m² or 25 kW/m². Therefore, it was determined from this mesh sensitivity test that grid sizes of about 0.15 mm and 1 mm on the radial and the longitudinal edges, respectively, are fine enough for discretizing the four bubble pumps.

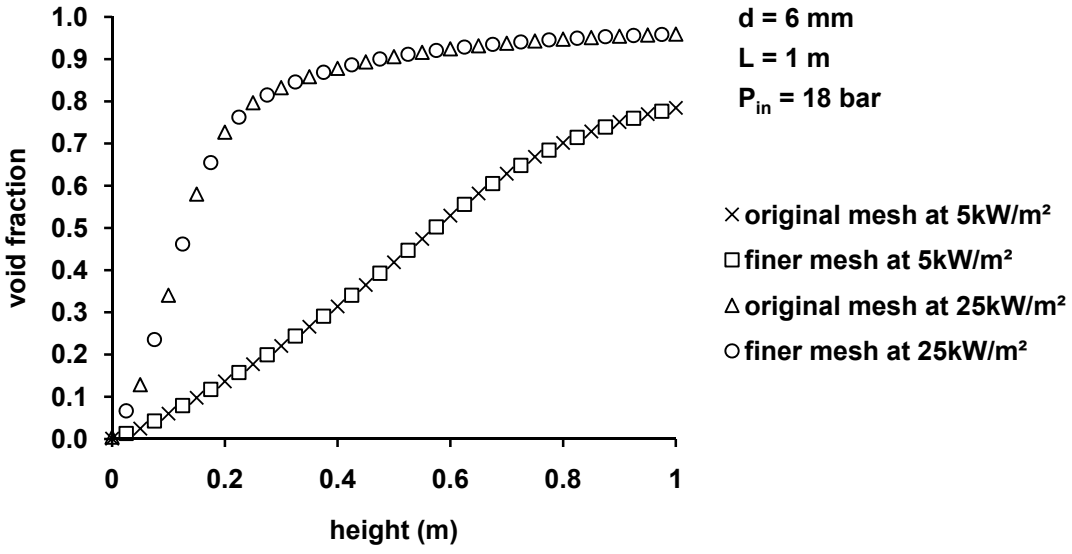

Figure 5-3. Void fraction comparison between the original mesh and the finer mesh

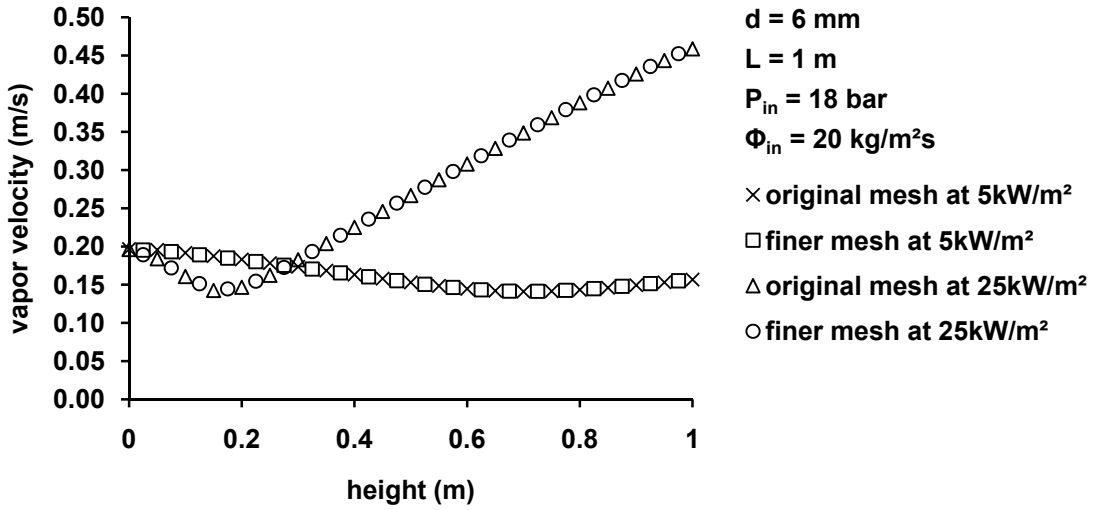

Figure 5-4. Vapor velocity comparison between the original mesh and the finer mesh

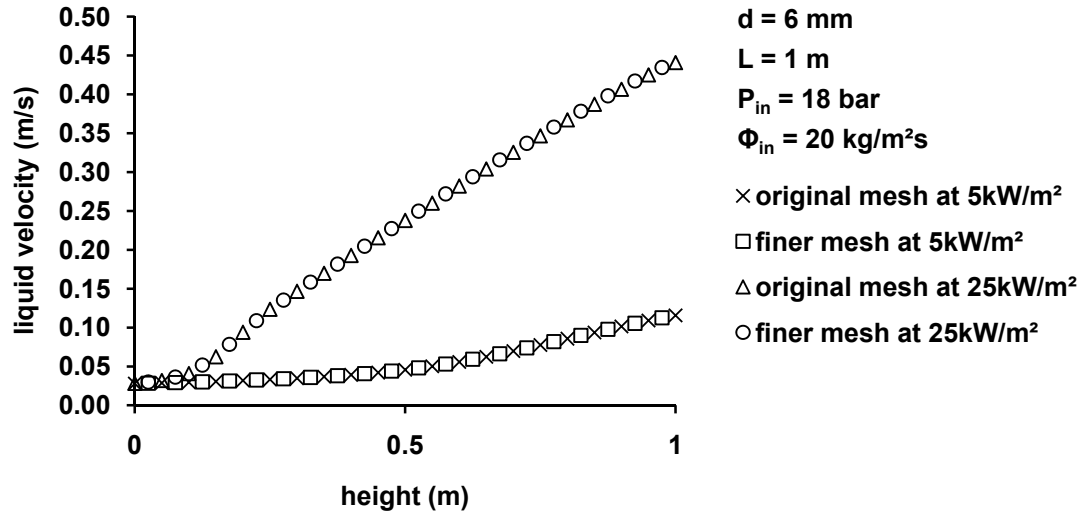

Figure 5-5. Liquid velocity comparison between the original mesh and the finer mesh

Validation of Numerical Model

Once the mesh sensitivity study is completed, validation of the present numerical model is needed. However, it is not yet feasible to check the applicability of the present numerical model for simulating bubble pumps due to the lack of physical data in an

actual bubble pump experiment using an ammonia-water solution for the working fluid as in the previous works [4, 6, 9-11].

Some efforts to examine the applicability of multi-dimensional numerical models for predicting the boiling two-phase flow in a vertical pipe having a uniform heat flux boundary condition along the pipe wall are found in the literature [14, 15, 21], where the numerical predictions were compared to the experimental data of Bartolomei and Chanturiya [22]. The comparisons were made for the flow parameters of the vertical pipe in terms of only the area-averaged void fraction distribution in the longitudinal direction and the liquid temperature distribution in the radial direction.

Lai and Farouk [14] showed that their numerical simulations using k-epsilon turbulence model for liquid phase were in a reasonable agreement with the experimental data.

Wintterle [15] investigated the applicability of the k-epsilon turbulence model using the wall function method for the two-phase flow when the void fraction gradient normal to the wall is high. To test the correct implementation of the wall function for the two-phase k-epsilon turbulence model, he verified the void fraction and temperature profiles for the two-phase flow which was implemented in the CFX code. It was confirmed that the results were decent for the two-phase flow case. The void fraction distributions along the pipe were shown to be predicted well, but the wall temperature in the radial direction was predicted 10-20 K higher than the experimental data [22].

Krepper et al. [21] also showed that the boiling model implemented in the CFX code is able to predict the area-averaged void fraction in the vertical heated tube with a reasonable agreement to the experimental data [22].

Based on the previous investigations [14, 15, 21], it seems practicable to use the k-epsilon turbulence model adopting the wall function method for predicting boiling flow in a vertical circular pipe although the accuracy could not be comprehensively checked due to the lack of available experimental data of the void fraction distributions in the radial direction.

The experimental model [22] is similar to the bubble pump model under consideration in the present study except that the fluid entering the vertical pipe is compressed water whereas saturated ammonia-water solution enters the bubble pump in the present study. Therefore, the experimental data [22] are used as a countermeasure in this study to confirm if the numerical schemes and mesh model implemented in the present CFX code are applicable to the bubble pump simulations.

Because the object here is to validate the modeling methods for simulating a bubble pump, few simulation cases in references [14, 15] are replicated and compared with the existing experimental data [14, 15, 22]. Two cases are simulated first to obtain void fraction profiles in the longitudinal direction, and the results are compared to the experimental data.

Mass, momentum, and energy conservation equations are applied for each of the two non-equilibrium phases. Turbulent flow of the liquid phase is simulated using the standard k-epsilon model adopting the wall function method.

Experimental data of void fraction profiles in the longitudinal direction and temperature distributions in the radial direction are compared with the calculations obtained by implementing the present numerical schemes in the CFX code. Figures 5-6

and 5-7 are the profiles of cross-sectional area-averaged void fraction obtained from replicating the simulations.

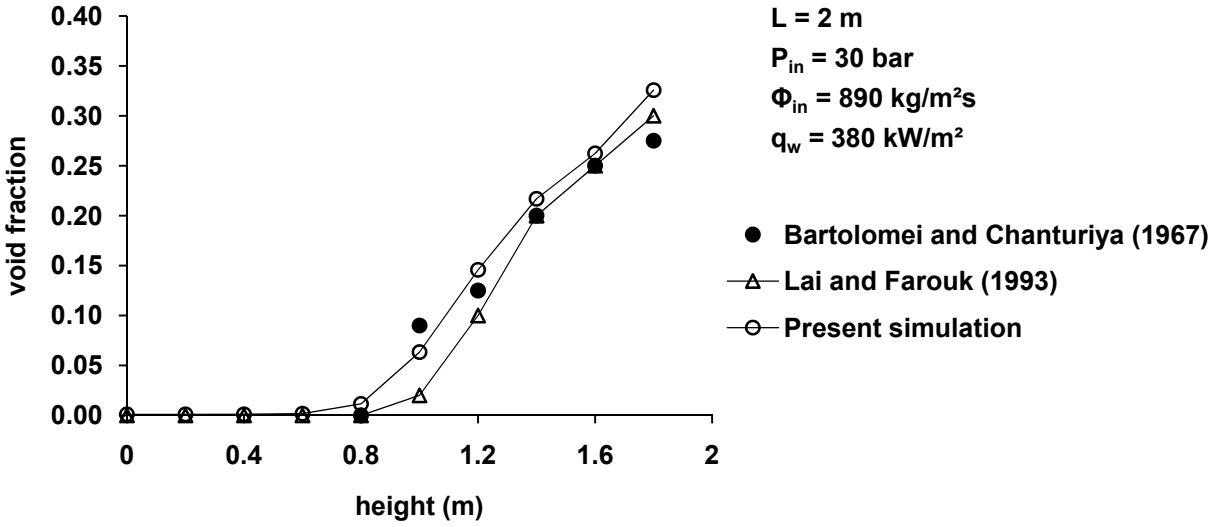

Figure 5-6. Comparison between the predicted and measured void fraction profiles in Case 2a

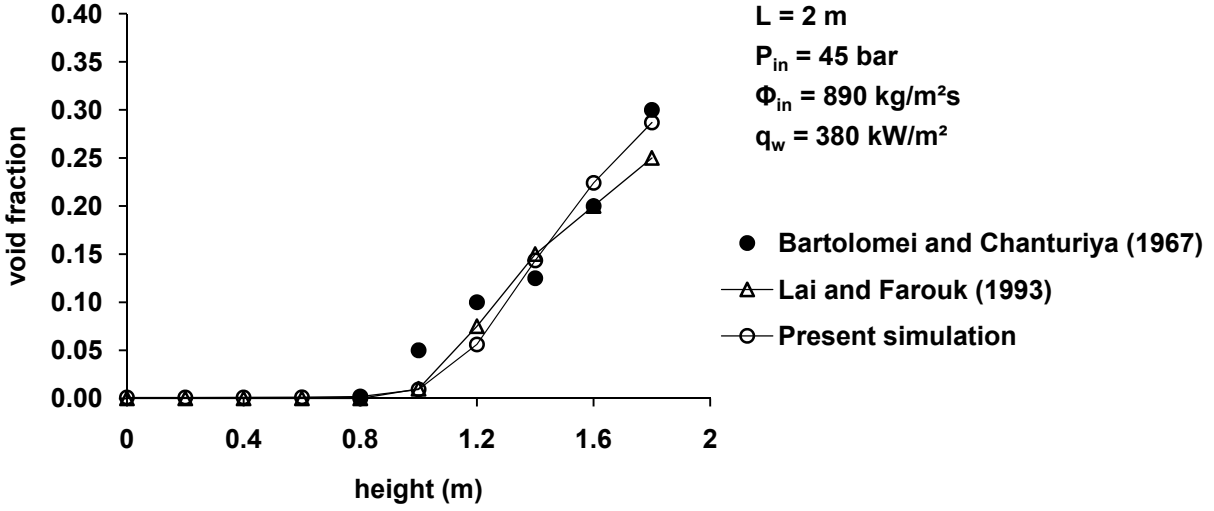

Figure 5-7. Comparison between the predicted and measured void fraction profiles in Case 3a

Correlating Figures 5-6 and 5-7 to Figures 13(b) and 13(c) in reference [14] respectively, the differences between the simulated results of this study and the

experimental results of Bartolomei and Chanturiya [14, 15, 22] seem to be within reasonable agreement. However, the difference in void fraction between the simulated results and the experimental results can go up to about 0.05.

In addition, the calculation results of the temperature distributions in the radial direction at two different levels are compared to the experimental data, as shown in Figures 5-8 and 5-9.

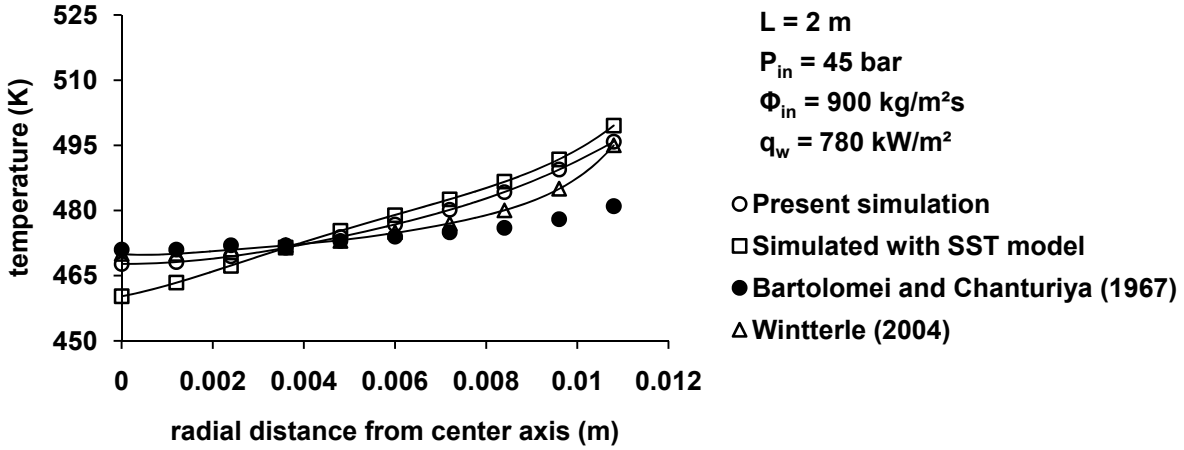

Figure 5-8. Comparison between the predicted and measured temperature profiles at 0.82 m height in Case II

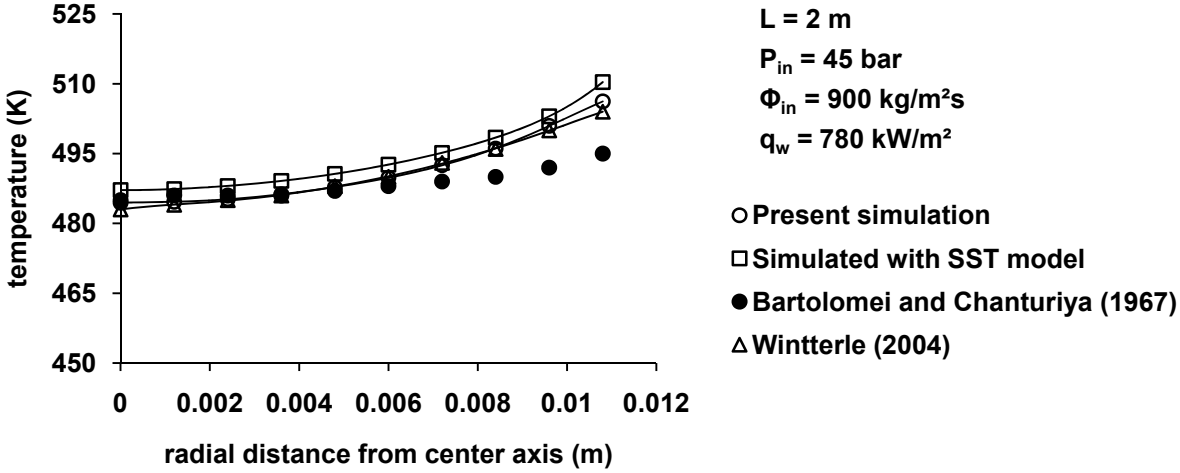

Figure 5-9. Comparison between the predicted and measured temperature profiles at 1.22 m height in Case II

Correlating Figures 5-8 and 5-9 to Figures 6.6 and 6.7 in reference [15] respectively, the differences between the simulation results of this study and the experimental results of Bartolomei and Chanturiya [14, 15, 22] seem to be within certain ranges of uncertainty overall. However, it is observed from Figures 5-8 and 5-9 that the simulated temperature distributions near the wall in the radial direction are higher than the experimental measurements, showing steeper gradients. The differences in temperature near the wall can be as large as 15K.

To further examine the applicability of the wall function method in treating the boundary layer for the simulation of the present boiling flow problem, a comparison is made between the SST turbulence model using a mesh with a very fine grid in the near-wall region as shown in Figure 5-10 and the standard k-epsilon turbulence model adopting the wall function method for the liquid phase.

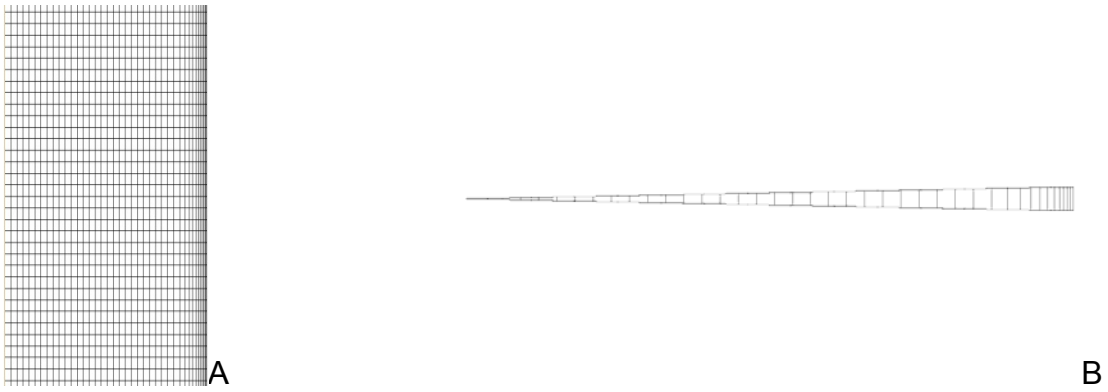

Figure 5-10. Mesh with a very fine grid in the boundary layer. A) Front view. B) Top view.

Figures 5-8 and 5-9 show that the SST turbulence model with a very fine grid in the boundary layer does not seem to provide any further improvement of accuracy in predicting the temperature distributions in the radial direction compared to k-epsilon model using the wall function method. Consequently, the temperature distributions in

the radial direction resulted from the both simulations deviate from the experimental data, especially in the near-wall region.

Thus, it is considered that the present code model has some shortcomings in simulating the boiling phase change and flow in the vertical pipe with accuracy. The shortcomings seem to be originated from the problems as discussed below.

The present simulation uses the k-epsilon turbulence model with the wall function method for the treatment of liquid flow in the near-wall region. Because of vapor generation near the wall, the boundary layer resolved by the wall function is not accurate. Furthermore, the near-wall region is not the only region affected by the inaccuracy in the fluid transport modeling since bubble growth pushes liquid from the wall region into the center, then affecting the whole flow field. In addition, bubble growth stirs the fluid, as does the unsteadiness, with effective turbulent viscosities higher by an order of magnitude than those of single phase turbulent boundary layers [23].

The present numerical model calculates only the void fraction instead of microscopically simulating the formations and behaviors of bubbles such as collision, coalescence, or breaking-up. Any of the turbulence closure methods cannot accurately simulate the bubble formation and behaviors which significantly change the momentum and transport rates [23].

Even the advanced turbulence modeling technique such as Large Eddy Simulation (LES), Detached Eddy Simulation (DES), etc. would not be adequate due to the same limitations that the two-equation turbulence models such as the k-epsilon and SST models have [23].

Thus, the formation and development of bubbles should be simulated by a very small time step-transient calculation method employing either any of the highly accurate simulation methods such as Direct Numerical Simulation (DNS) or any of the advanced methods that explicitly track the phase interfaces and apply different models in the liquid and gas phases. Alternatively, a single-phase turbulence model may be employed with a method adjusting the parameters so that the transport rates are somewhat close to experiment as a practicable way to approximately simulate the boiling phase change [23]. Also, the simulation domain fully covering a complete bubble pump is needed to obtain more accurate results than the simplified domain modeled in this study.

As these approaches can incur excessive computational cost or have technical limitations at present, there is little published literature addressing these applications to the practical engineering problems to the author's best knowledge.

To avoid the difficulties related to unaffordable computation costs and technical limitations which are accompanied by the use of such highly accurate simulation methods, the present study calculates the void fraction distribution using the k-epsilon turbulence model with the wall function method alternatively.

Based on the discussions above, it is concluded that the adoption of the present modeling method using the CFX code for simulating boiling phase change flow in a bubble pump is practical because it is ideally a circular tube in which ammonia vaporizes from the ammonia-water solution.

CHAPTER 6
RESULTS AND DISCUSSION

Output data obtained from the simulations are shown and analyzed in this chapter. Some results are compared to those of Benhmidene et al. [11], and their differences are examined. In addition, the applicability of the present numerical model to designing a bubble pump is discussed.

Before the results are presented, some issues concerning the accuracy of the results need to be described. Since experimental data of bubble pump are not available for comparison, the accuracy of the results cannot be fully examined. Nevertheless, the numerical modeling used in this study is seen to be capable of simulating two-phase flow decent and suitable for the macroscopic flow simulation considering the validation tests described in the previous chapter.

Flow Situation

An ammonia-water solution is vaporized in a bubble pump due to heating at the saturation temperature of the solution, which is dependent on both the ammonia concentration and the pressure. Because the boiling temperature of ammonia is significantly lower than that of water, only ammonia vaporizes from the solution while water remains in the solution. As ammonia vaporizes at constant pressure, the boiling temperature of the remaining solution rises because of the decreasing ammonia concentration.

The solution flowing into the bubble pump inlet as shown in Figure 4-1 is assumed to be saturated liquid as defined by the problem statement. Part of the heat transferred to the solution from the tube wall is used to vaporize the ammonia from the solution, while the remainder is used as sensible heat to increase the temperature of the solution

in which the ammonia concentration decreases. The buoyancy force created by the ammonia vapor in the solution acts as pumping force to move the solution upwards in the bubble pump.

Results from the numerical simulations of Pump D whose inside diameter is 12 mm subjected to a uniform heat flux of 5 kW/m², 15 kW/m², or 25 kW/m² are presented in terms of liquid (ammonia-water solution) and vapor (ammonia) velocities along with void fraction of the fluid (ammonia-water solution and ammonia vapor) flowing upwards through the bubble pump.

Figures 6-1 and 6-2 present the liquid and vapor velocity distributions on a symmetric vertical plane of the bubble pump model in contour and vector forms, respectively. In Figure 6-2, five local parts of the vertical plane at different heights are selected to clearly show typical local flow situations.

As shown in Figures 6-1 and 6-2, the liquid and vapor velocities generally increase from the pump inner region to the outer region in the radial direction as well as from the inlet to the outlet in the longitudinal direction. This is because the pump wall is subjected to a uniform heat flux along the pump length. The initial velocity of the vapor obtained by rapid local vaporization of ammonia near the wall decreases along the pump length to a certain height due to the gravitational force acting on the fluid and then increases after gaining enough buoyancy force. The figures show that the higher heat flux results in a higher fluid velocity and a greater radial velocity gradient.

The vapor velocity is shown to be greater than that of the liquid. However, the difference in velocities between the liquid and vapor is shown not to be significant due

to the larger buoyancy force acting on the liquid even though the liquid is much heavier than the vapor.

In Figure 6-2, a stagnant or reverse flow field of the liquid is found in the inner region when the fluid has not received enough heat to lift the liquid. As the fluid receives heat while flowing in the tube, a stagnant or reverse flow field becomes smaller since buoyancy force to overcome the gravitational force is becoming larger.

Along the entire length of the bubble pump, less heat reaches the inner region than the outer one. Therefore, the velocities of the liquid and vapor near the wall are higher than those in the inner region along the entire pump length.

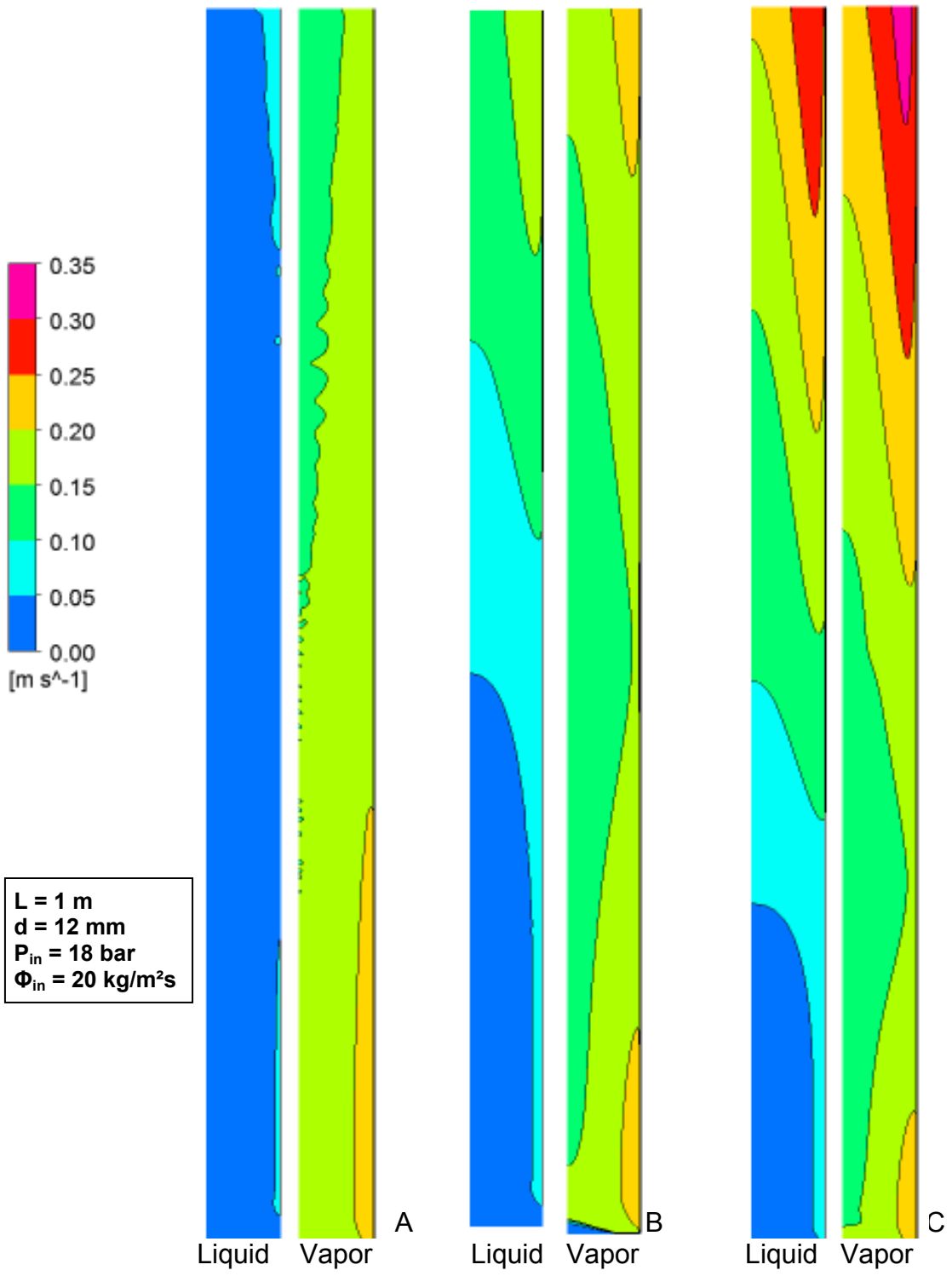

(Enlarged 10 times in the radial direction, the right side of each drawing is the wall.)

Figure 6-1. Liquid and vapor velocity contours in Pump D subjected to a uniform heat flux of A) 5 kW/m², B) 15 kW/m² or C) 25 kW/m² from the wall

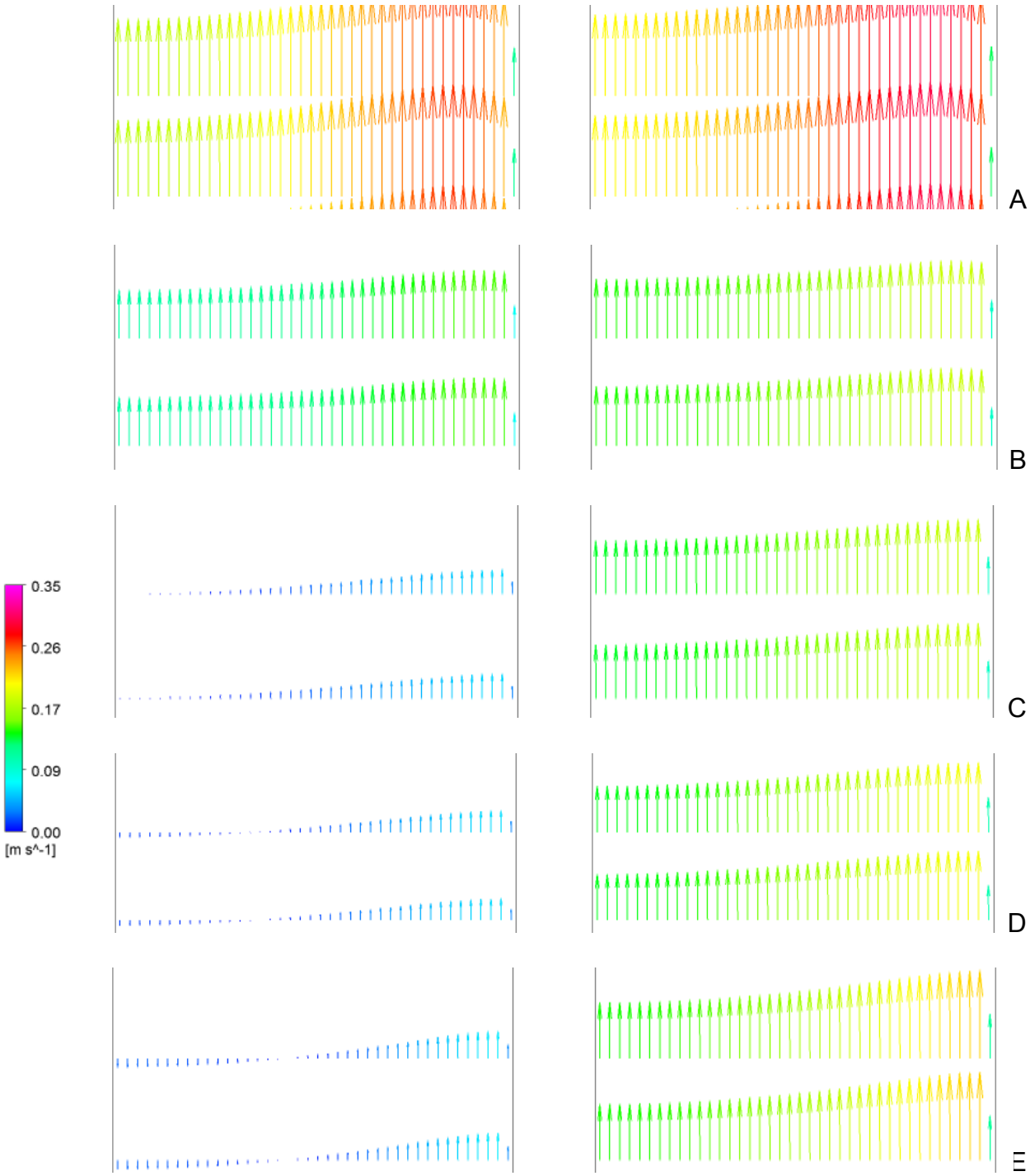

Figure 6-2. Liquid and vapor velocity vectors at five different heights of A) 0.9 m, B) 0.5 m, C) 0.15 m, D) 0.1 m and E) 0.05 m in Pump D subjected to a uniform heat flux of 25 kW/m² from the wall

Void Fraction

Void fraction refers to the fraction of the volume occupied by the vapor phase, so the void fraction distributions are examined to see how much of the binary solution has transformed to the vapor phase along the vertical length of the bubble pump.

Figure 6-3 shows void fraction distributions of the fluid on the symmetric vertical plane of Pump D subjected to a uniform heat flux of 5 kW/m², 10 kW/m², 15 kW/m², 20 kW/m² or 25 kW/m². It is shown that the void fraction of the fluid increases along the longitudinal direction from the inlet to the outlet. The radial variation of the void fraction in the pump subjected to small heat flux is steep. This implies that heat is hardly transferred to the fluid flowing in the inner region of the pump when the amount of heat flux is small.

It is confirmed from Figure 6-3 that ammonia vaporization from the solution occurs more actively in the outer region near the wall than in the inner region as discussed previously. In addition, it is shown that the vaporization of ammonia slows down when the void fraction reaches about 0.8. This is because the boiling temperature of the solution increases as the concentration of ammonia in the solution decreases. Similar boiling flow situation in the bubble pumps as discussed above are found in references [24-26].

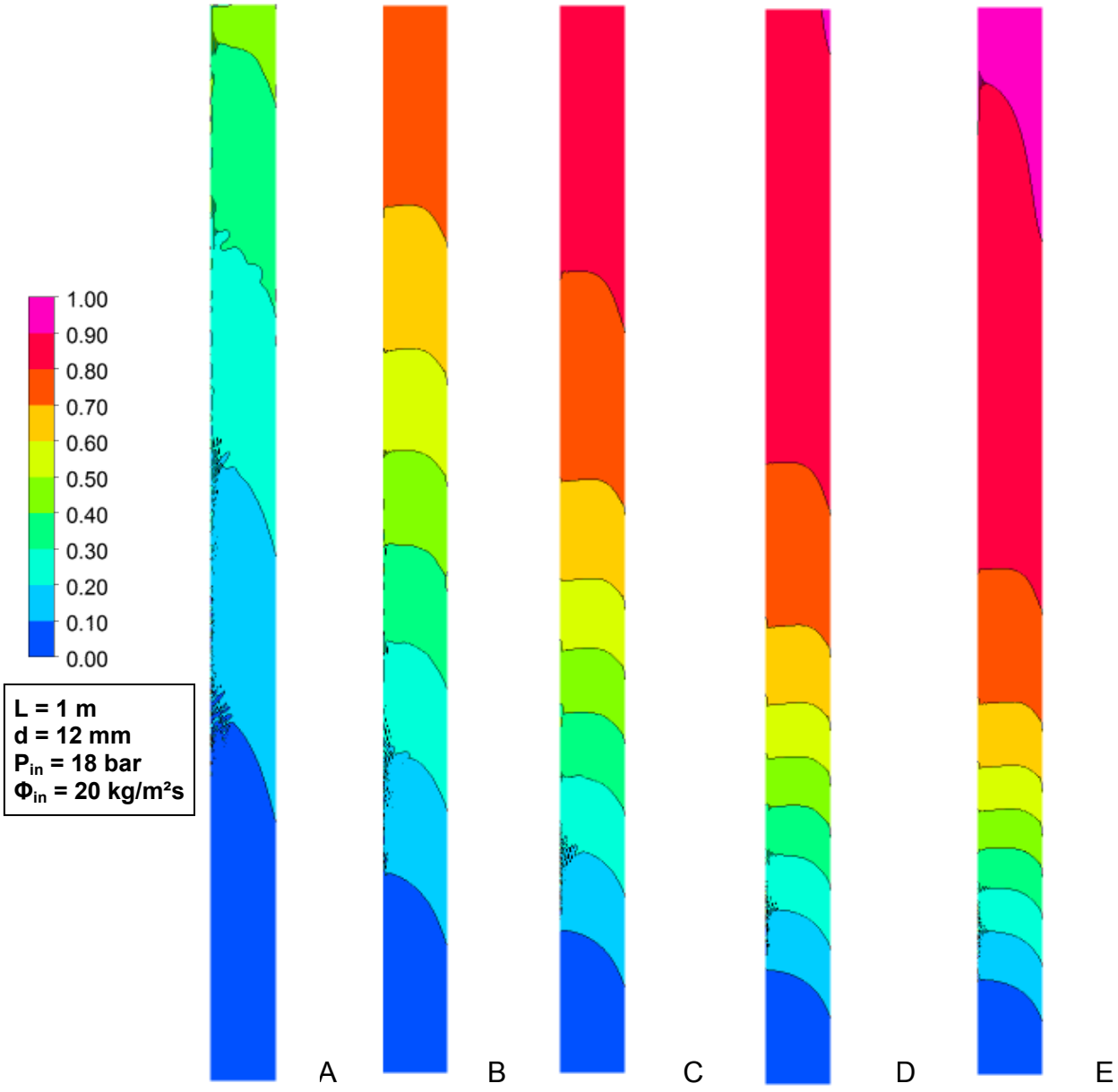

(Enlarged 10 times in the radial direction, the right side of each drawing is the wall.)

Figure 6-3. Void fractions in Pump D subjected to a uniform heat flux of A) 5 kW/m², B) 10 kW/m², C) 15 kW/m², D) 20 kW/m² or E) 25 kW/m² from the wall

Figures 6-4 and 6-5 show comparisons between the void fraction distributions simulated by the present model and those by the 1-D model [11] for Pumps A and D, respectively. The void fraction profiles of the present numerical simulations presented in this study are different from those of Benhmidene et al. [11]. The void fractions along the pump length obtained in the present study are generally lower than those in the literature [11].

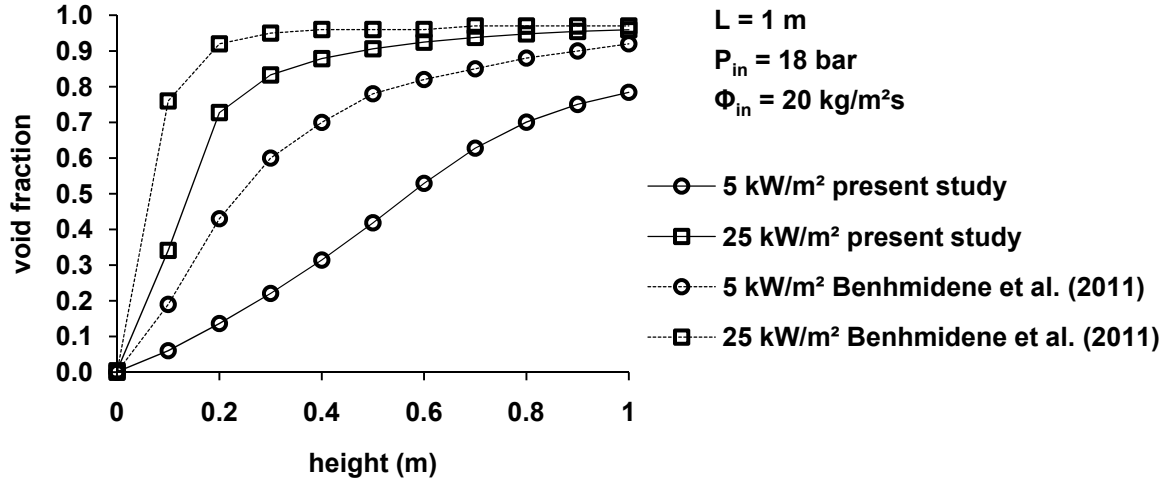

Figure 6-4. Comparison of void fraction between the present model and the 1-D model [11] for Pump A (6 mm)

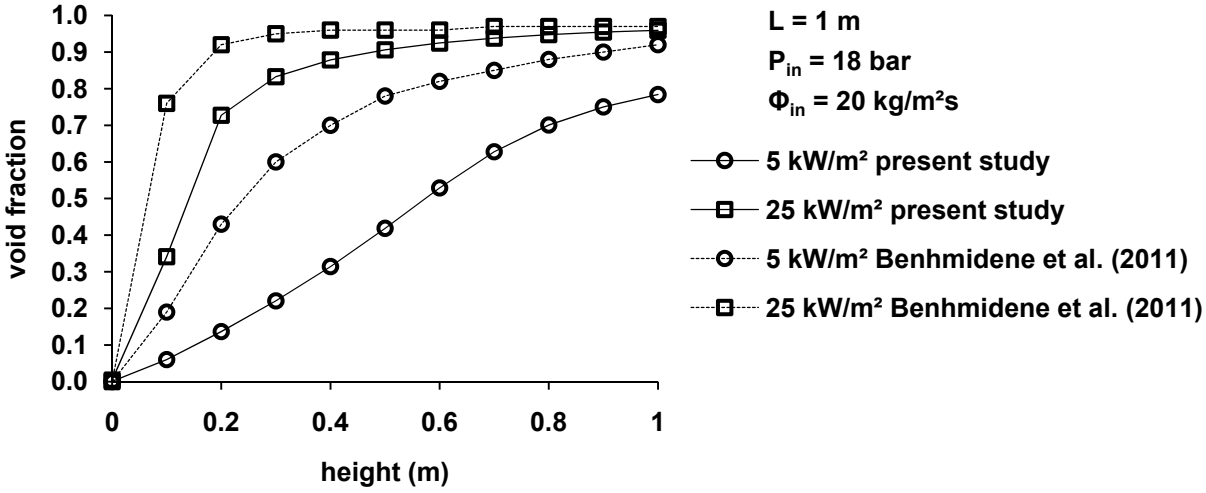

Figure 6-5. Comparison of void fraction between the present model and the 1-D model [11] for Pump D (12 mm)

To investigate the influence of the pump diameter and the heat flux on the void fraction, cross-sectional area-averaged void fraction profiles are shown for the four pumps under five amounts of heat flux as shown in Figures 6-6 through 6-9.

In Figures 6-6 through 6-9, it can be observed that the void fraction increases as the fluid rises through the pump, which means that more ammonia-water solution boils as it travels in the pump. As the pump diameter decreases or the heat flux increases, the void fraction converges faster to a maximum value. Because the initial ammonia concentration of the solution is 40%, the maximum void fraction of 0.986 can be attained when the ammonia component evaporates completely. As shown in the above figures, the void fraction does not reach 0.986 in any of the 20 cases tested. The case where the void fraction at the outlet is lower than the maximum value means that ammonia does not completely vaporize from the ammonia-water solution. Therefore, the weak ammonia-water solution that is low in ammonia concentration exits the bubble pump outlet along with the ammonia vapor.

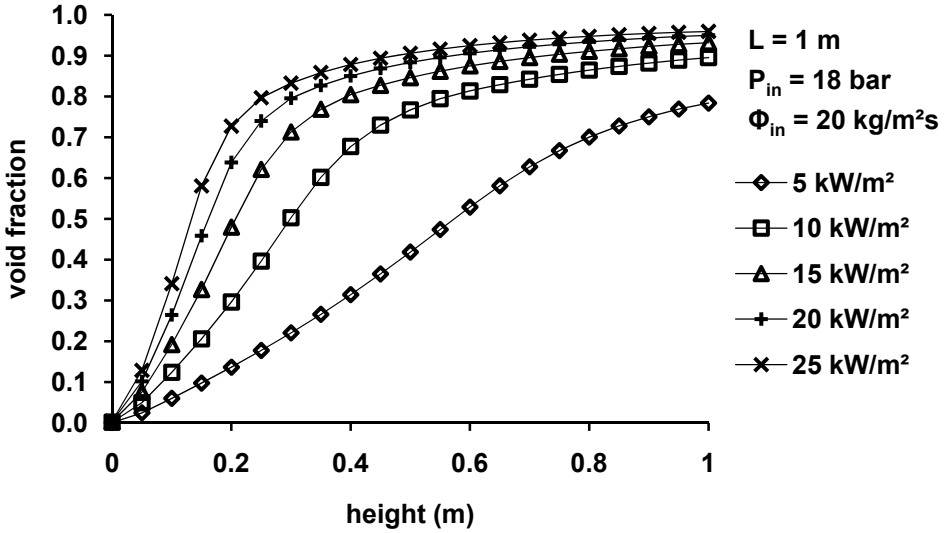

Figure 6-6. Void fraction profiles for Pump A (6 mm)

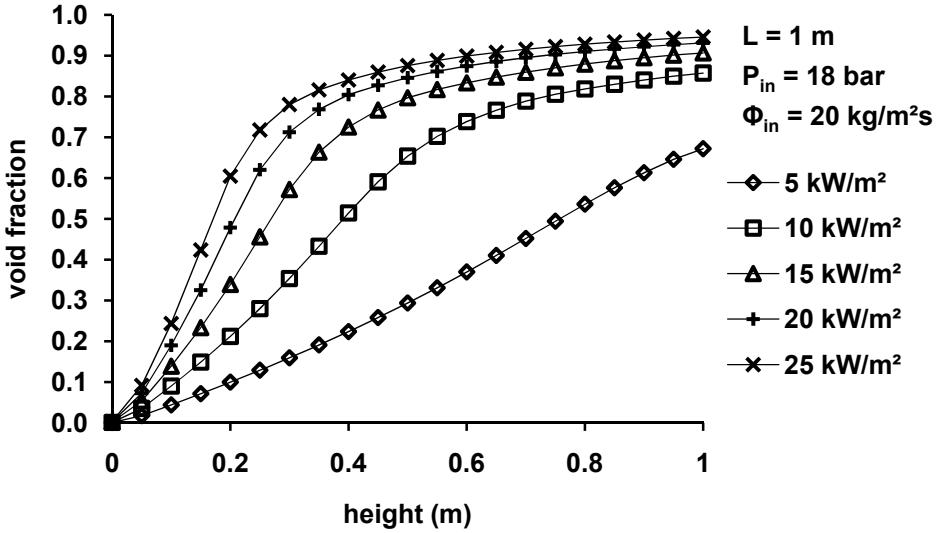

Figure 6-7. Void fraction profiles for Pump B (8 mm)

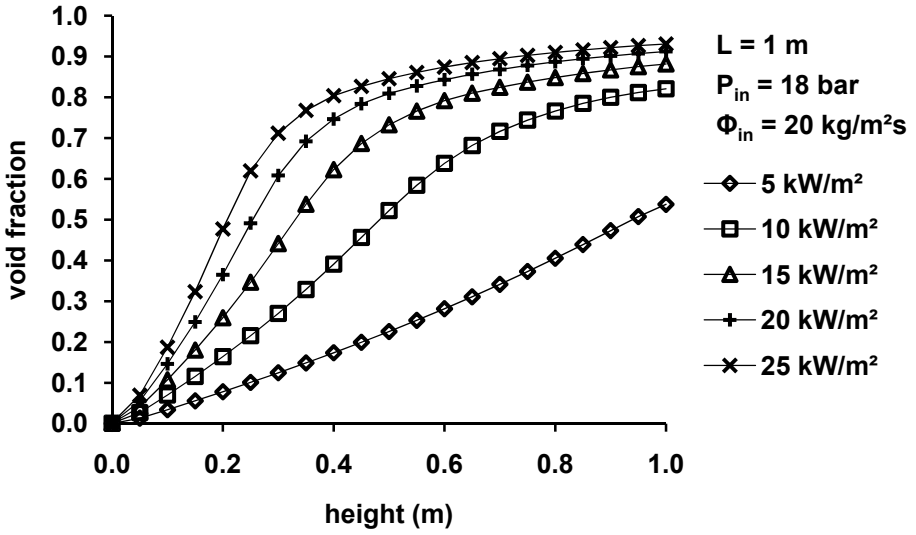

Figure 6-8. Void fraction profiles for Pump C (10 mm)

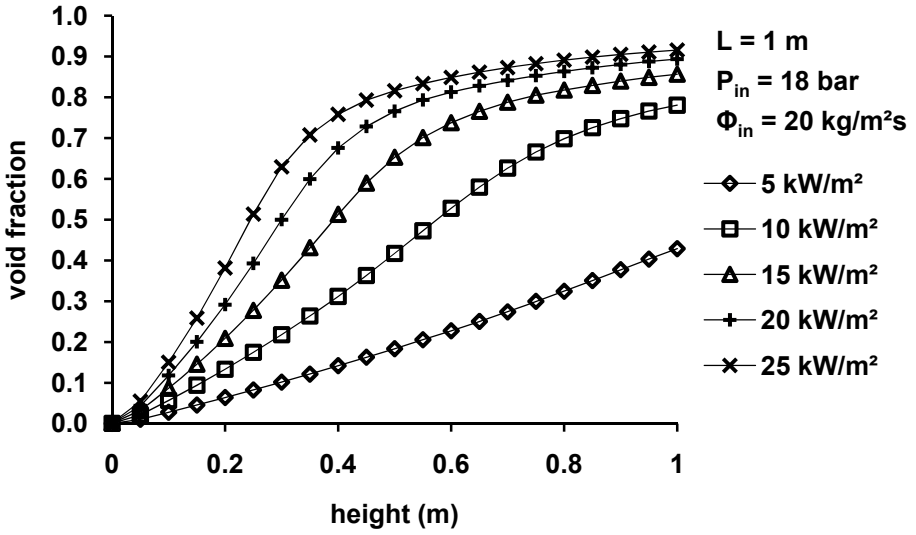

Figure 6-9. Void fraction profiles for Pump D (12 mm)

Slip Ratio

The slip ratio is defined as the ratio of vapor (ammonia) velocity to liquid (ammonia-water solution) velocity in the tube. The inverse of slip ratio is referred as pumping ratio of bubble pump in few references [10, 11].

Figures 6-10 through 6-13 show cross-sectional area-averaged vapor velocity with respect to cross-sectional area-averaged liquid velocity for the four pumps under five amounts of heat flux. From the figures, it is seen that if the diameter is smaller or the heat flux is greater, the liquid and vapor velocities are higher. This behavior is due to the increase in the amount of heat flux per unit volume of the fluid.

It can also be seen from the aforementioned figures that vapor velocity initially decreases while the void fraction rapidly increases. This is most likely due to the stagnant or reverse liquid flow found in the inner region of bubble pump when not enough buoyancy is created by the vapor to lift up the liquid in the inner region as observed in Figure 6-2. The stagnant or reverse liquid flow interferes the vapor from gaining streamwise velocity. Most of the thermal energy received from the wall is used for phase change which results in a rapid void fraction increase. Once enough ammonia vapor to make the buoyancy force acting on the fluid greater than the gravitational force is formed, both the liquid and vapor velocities increase. The thermal energy transferred from the wall is used for the continuous phase change of the solution and for the heat-up of both the solution and the vapor. It is observed that the vapor velocity increases rapidly when the void fraction reaches about 0.7.

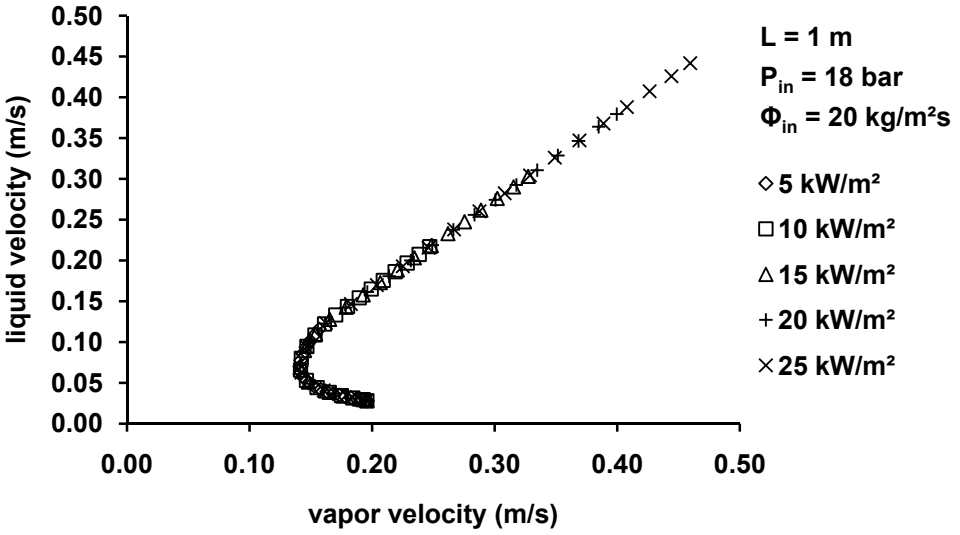

Figure 6-10. Liquid velocity vs. vapor velocity for Pump A (6 mm)

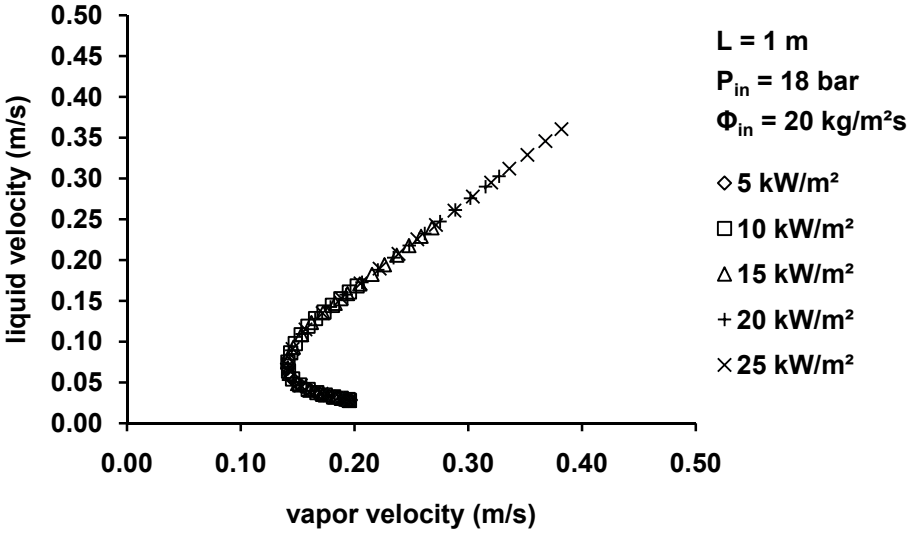

Figure 6-11. Liquid velocity vs. vapor velocity for Pump B (8 mm)

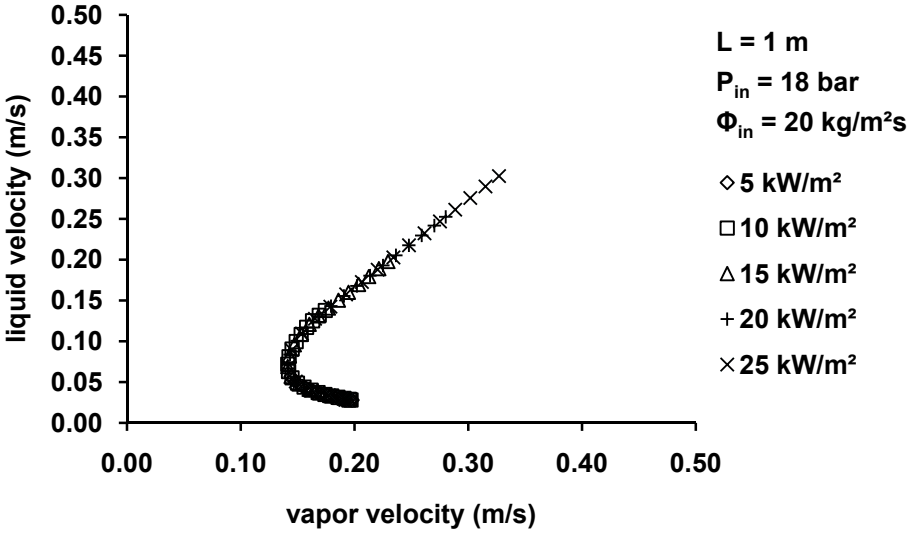

Figure 6-12. Liquid velocity vs. vapor velocity for Pump C (10 mm)

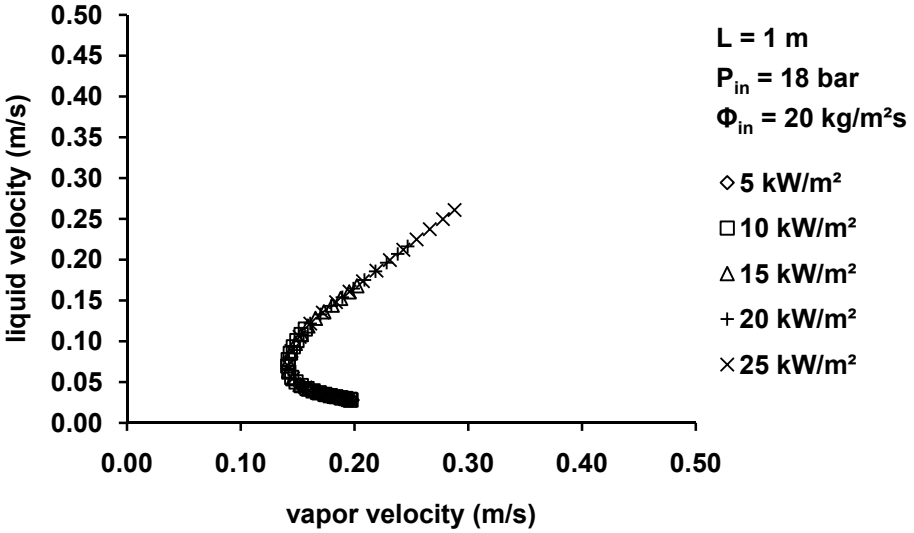

Figure 6-13. Liquid velocity vs. vapor velocity for Pump D (12 mm)

Figure 6-14 shows the slip ratios at the outlet simulated by the present model for four pumps with different diameters. The present simulations show that the outlet slip ratio decreases either as the heat flux increases or as the diameter decreases meaning that the liquid is pumped better. A bubble pump with a larger diameter is supposed to be less efficient at pumping the liquid due to the larger resistance to heat transfer in the radial direction, as discussed previously. Therefore, the slip ratio is lower with a smaller diameter which implies that the liquid flows nearly as fast as the vapor. Also, increasing heat input creates a larger buoyancy force which should further accelerate the liquid.

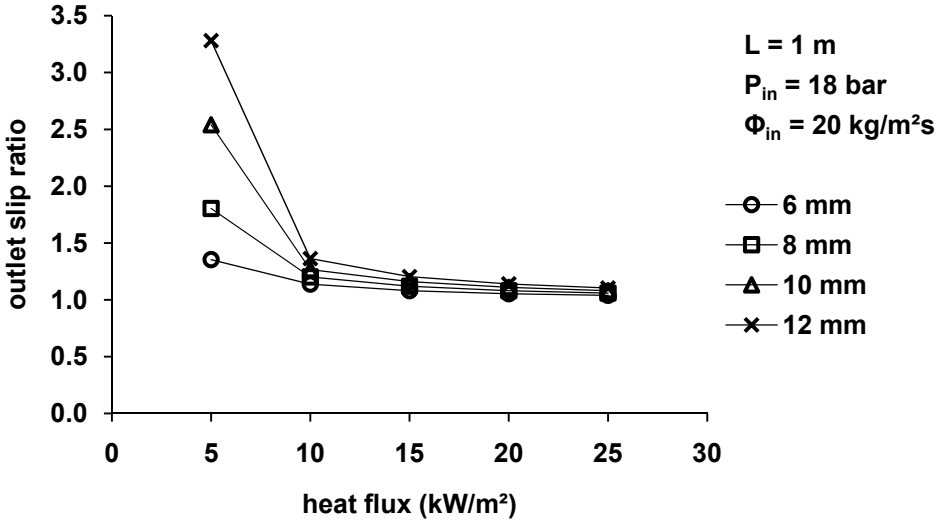

Figure 6-14. Outlet slip ratio of the present model for four different pumps

Figures 6-15 and 6-16, respectively, show the slip ratio variations along the pump length simulated by the present model for Pumps A and D under five amounts of heat flux. As shown, the slip ratio generally decreases as the fluid flows upwards along the pump length and also as the amount of heat flux increases. Comparing both cases of Pumps A and D, it is seen that the slip ratio in Pump A (with smaller diameter) decreases faster and more steeply than in Pump D (with larger diameter) under the condition that the mass flux of the ammonia-water solution is constant at the pump inlet.

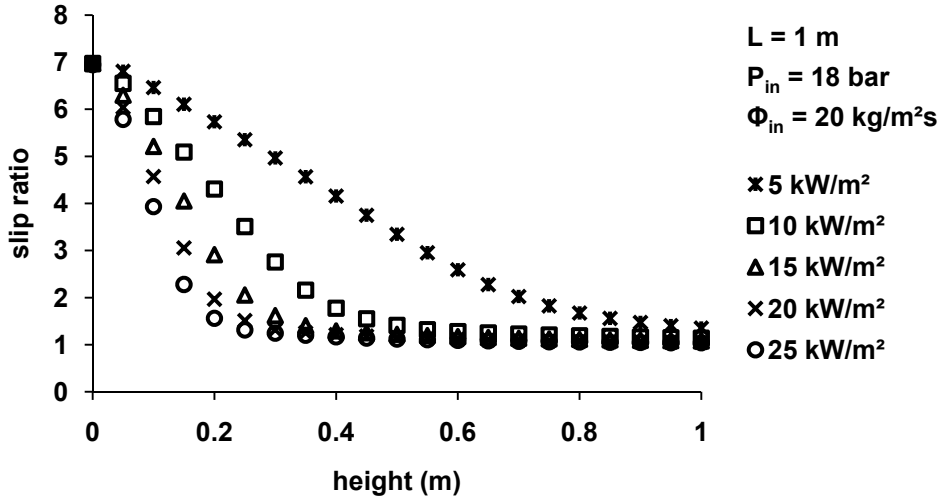

Figure 6-15. Slip ratio profiles for Pump A (6 mm)

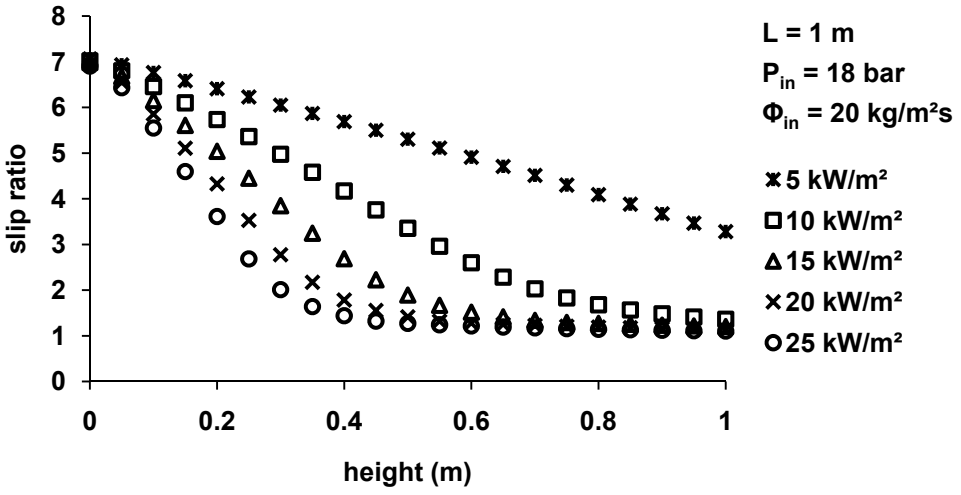

Figure 6-16. Slip ratio profiles for Pump D (12 mm)

Based on the above discussion, some background information for designing a bubble pump can be estimated. For example, the required minimum length of a bubble pump design with a diameter of 6 mm and an outlet slip ratio of 1.1 can be determined from Figure 6-15 to be about 0.5 m for a heat flux of 25 kW/m², while about 0.75 m of length is appropriate for a heat flux of 15 kW/m². Similarly, the background information and knowledge for the optimum design of a bubble pump can be obtained from the present numerical simulations. Finally, it is considered that the simulations can be done for various inlet or boundary conditions such as specifying a constant mass flow rate at the inlet rather than a constant mass flux. Otherwise, a non-uniform periodic heat flux can be specified or different geometrical configurations having an inclined geometry and/or a thick wall can be defined as well.

CHAPTER 7
CONCLUSIONS AND RECOMMENDATIONS

This study examined a numerical model of flow in a bubble pump subjected to a uniform heat flux. The simulations of bubble pumps were implemented using a commercial CFD code. The applicability of the numerical model for the bubble pump simulations, which was implemented in the CFD code, was examined by conducting simulations of a subcooled boiling induced two-phase upwarding flow in a vertical pipe subjected to a uniform wall heat flux for which the experimental data are available.

For the present numerical simulations, both the standard k-epsilon turbulence model and the algebraic (zero-equation) turbulence model were used for the continuous liquid phase and dispersed gas phase flows, respectively.

To investigate the influences of the pump diameter and the amount of heat flux on the physical operating conditions of a bubble pump, a total of 20 simulation cases were considered by adapting four bubble pumps with different diameters for the cases where each pump wall is subjected to five amounts of heat flux. Typical simulation results of the bubble pump flow parameters were presented and the influences of bubble pump diameter and heat flux on these parameters were discussed in detail. The key findings derived from this study can be summarized as follows.

It is seen that the k-epsilon turbulence model with the wall function method cannot accurately simulate the boiling flow situation in the radial direction in a vertical heated pipe, but predicts the longitudinal distributions of the cross-sectional area-averaged flow parameters reasonably well as found in the previous studies.

Little difference is found between the two numerical simulations of the boiling flow in the vertical heated pipe using either the standard k-epsilon model with the wall function method or the SST model with a very fine grid in the near-wall region.

To accurately simulate the boiling flow in a heated vertical pipe, the formation and development of bubbles should be modeled by a small time-step transient calculation employing either any of the highly accurate simulation methods such as DNS or any of the advanced methods that explicitly track the phase interfaces and apply different models in the liquid and gas phases. Alternatively, an improved single-phase turbulence model may be employed with the method adjusting the parameters so that the transport rates are somewhat close to experiment as a practicable way to approximately simulate the boiling phase change.

Even in the case of employing any of the available advanced methods for the simulation of boiling flow in a heated vertical pipe, it would be necessary to conduct precise experiments for comprehensively assessing the accuracy of the numerical simulation.

Nevertheless, the numerical model used in this study can be useful for predicting the void fraction and velocity distributions in the bubble pumps for certain industrial applications practically although it has some inherent shortcomings in simulating boiling turbulent flow in a heated vertical pipe as discussed previously.

The present numerical simulation results show that higher heat flux and smaller diameter provide better boiling condition in the bubble pumps so that the outlet slip ratio decreases as either the heat flux increases or the diameter decreases. In addition, other background information for drafting the design of a bubble pump can be inferred from

the CFD calculations using the present numerical model. However, supporting experimental tests need to be done for evaluating the present numerical model.

LIST OF REFERENCES

[1] Wang, X., and Chua, H. T., 2009, "Absorption Cooling: A Review of Lithium Bromide-Water Chiller Technologies," Recent Patents on Mechanical Engineering, **2**(3), pp. 193-213.

[2] Srikhirin, P., Aphornratana, S., and Chungpaibulpatana, S., 2001, "A Review of Absorption Refrigeration Technologies," Renewable and Sustainable Energy Reviews, **5**(4), pp. 343-372.

[3] Dannen, G., 1997, "The Einstein-Szilárd Refrigerators," Scientific American, **276**(1), pp. 90-95.

[4] White, S. J., 2001, "Bubble pump design and performance," Georgia Institute of Technology, Atlanta, GA.

[5] De Cachard, F., and Delhaye, J., 1996, "A Slug-Churn Flow Model for Small-Diameter Airlift Pumps," International Journal of Multiphase Flow, **22**(4), pp. 627-649.

[6] Shelton, S. V., Stewart, S. W., and Erickson, D., 2002, "Bubble Pump Design for Single Pressure Absorption Refrigeration Cycles," ASHRAE Transactions, **108**(1), pp. 867-876.

[7] Koyfman, A., Jelinek, M., Levy, A., 2003, "An Experimental Investigation of Bubble Pump Performance for Diffusion Absorption Refrigeration System with Organic Working Fluids," Applied Thermal Engineering, **23**(15), pp. 1881-1894.

[8] SATHE, A., 2001, "Experimental and Theoretical Studies on a Bubble Pump for a Diffusion Absorption Refrigeration System," India Institute of Technology, Madras, India.

[9] Dammak, N., Chaouachi, B., Gabsi, S., 2010, "Optimization of the Geometrical Parameters of a Solar Bubble Pump for Absorption-Diffusion Cooling Systems," American Journal of Engineering and Applied Sciences, **3**(4), pp. 693-698.

[10] Benhmidene, A., Chaouachi, B., Gabsi, S., 2011, "Modelling of Heat Flux Received by a Bubble Pump of Absorption-Diffusion Refrigeration Cycles," Heat and Mass Transfer, **47**(11), pp. 1-7.

[11] Benhmidene, A., Chaouachi, B., Bourouis, M., 2011, "Numerical Prediction of Flow Patterns in Bubble Pumps," Journal of Fluids Engineering, **133**(3)**,** pp. 031302.1-031302.7.

[12] ANSYS, 2011, “CFX USER MANUAL,” ANSYS Inc., Canonsburg, PA.

[13] Dewan, A., 2010, "*Tackling Turbulent Flows in Engineering*," Springer, Berlin, Germany.

[14] Lai, J., and Farouk, B., 1993, "Numerical Simulation of Subcooled Boiling and Heat Transfer in Vertical Ducts," International Journal of Heat and Mass Transfer, **36**(6), pp. 1541-1551.

[15] Wintterle, T., 2004, "Development of a numerical boundary condition for the simulation of nucleate boiling at heated walls," University of Stuttgart, Germany.

[16] Ferziger, J.H., and Perić, M., 2002, "*Computational Methods for Fluid Dynamics*," Springer, Berlin, Germany.

[17] Lucas, D., Tiselj, I., Hassan, Y. A., and Moretti, F., 2009, "Computational Fluid Dynamics for Gas-Liquid Flows," Science and Technology of Nuclear Installations.

[18] NIST, 2010, “REFPROP USER MANUAL,” National Institute of Standards and Technology, Gaithersburg, MD.

[19] ASHRAE, 2009, "*Handbook: Fundamentals*," American Society of Heating, Refrigerating and Air-Conditioning Engineers, Inc., Atlanta, GA.

[20] ANSYS, 2009, “Multiphase Flow Modeling in ANSYS CFX,” Training Manual for ANSYS CFX, ANSYS, Inc., Canonsburg, PA.[21] Krepper, E., Koncar, B., and Egorov, Y., 2007, "CFD Modelling of Subcooled Boiling--Concept, Validation and Application to Fuel Assembly Design," Nuclear Engineering and Design, **237**(7), pp. 716-731.

[22] Bartolomei, G., and Chanturiya, V., 1967, "Experimental Study of True Void Fraction when Boiling Subcooled Water in Vertical Tubes," Thermal Engineering, **14**(2), pp. 123-128.

[23] Lear, W. E., 2011, "Personal Communications with the Comments on a Draft of this Thesis."

[24] Ishii, M., and De Jarlais, G., 1987, "Flow Visualization Study of Inverted Annular Flow of Post Dryout Heat Transfer Region," Nuclear Engineering and Design, **99**, pp. 187-199.

[25] Johannsen, K., 1991, "Low Quality Transition and Inverted Annular Flow Film Boiling of Water: An Updated Review," Experimental Thermal and Fluid Science, **4**(5), pp. 497-509.

[26] Nakla, M. E., Groeneveld, D., and Cheng, S., 2011, "Experimental Study of Inverted Annular Film Boiling in a Vertical Tube Cooled by R-134a," International Journal of Multiphase Flow, **37**(1), pp. 67-75.

BIOGRAPHICAL SKETCH

Mr. Jo was born in South Korea. He earned dual bachelor's degrees in mechanical engineering and engineering physics from University of Michigan - Ann Arbor. He received a master's degree in mechanical engineering from University of Florida.